Optical and Magnetical Properties of Endohedral Silicon Cages

Mário Rui Gonçalves Marques

Department of Physics

University of Coimbra

Thesis Advisors:

Fernando Manuel da Silva Nogueira

Micael José Tourdot de Oliveira

A thesis submitted for the degree of

Master of Science

Coimbra, 14th July, 2015

I would like to dedicate this thesis to my loving parents ...

Acknowledgements

I would like to start thanking my supervisors, Dr. Fernando Nogueira and Dr. Micael Oliveira, for all the help and lessons they gave me. I learnt a lot.

I would like to thank my parents, I would not be here if not for them. To my mother for the amazing stories. To my father, all that page skipping sharpened my mind.

I would like to thank my favourite brother.

I would like to thank all my friends at the Physics Department.

Also, I would like to thank all the members of the Center for Computational Physics.

I would like to thank Maxwell-Boltzmann for their inspiration.

Finally, I would like to thank Blue for being there for me.

Abstract

This work shows a study of optical and magnetical properties of endohedral silicon cages containing transition metal atoms. Geometries with different magnetizations are calculated using density functional theory and the optical response of these systems is obtained by employing real-time, real-space time-dependent density functional theory. A comparison and discussion of the results is also present.

Resumo

Este trabalho mostra um estudo de propriedades ópticas e magnéticas de gaiolas endohédricas de silício contendo átomos de metais de transição. Geometrias para diferentes magnetizações são calculadas usando a teoria dos funcionais da densidade enquanto que a resposta óptica destes sistemas é obtida usando a teoria dos funcionais da densidade dependente do tempo em espaço real e em tempo real. Uma comparação e discussão dos resultados também é apresentada.

Contents

List of Figures

List of Tables

Part I

Introduction

Introduction

Until 1988's discovery of the giant magnetoresistive effect, the spin of the electron was completely ignored in electronic devices, based on electrons' charge. Currently, spintronics (spin based electronics) presents itself as an active field of work, which exhaustively seeks new methods and models with the intent of creating spintronic devices in the near future. The advantages of these devices would be nonvolatility, increased data processing speed, decreased electrical power consumption and increased integration densities compared with conventional semiconductor devices [1]. One of the ideas that lay around is the possibility to control the spin of a system using electric fields, since the spin-orbit interaction connects the charge and spin dynamics of a system [2, 3]. In fact, this thesis is a continuation of the work done in [3]. Imagine a building block that could be in any of two stable states, each characterised by a different magnetization and let an electrical field be able to change one state to the other. If each magnetization state is associated with one number, 0 or 1, this could be the building block of an hard disk.

The main objective of this work is to find endohedral silicon cages with different structures, due to a different magnetization of the system and then, investigate if these different structures can be identified by their photo-absorption spectrum. Here endohedral is used based on its etymology, meaning there is something inside the structure, in this case, an atom, a molecule or a cluster of a transition metal inside the silicon cage. To achieve a solution of this many-body problem density functional theory (DFT) and time-dependent density functional theory (TDDFT) will be used. While DFT permits to describe the ground state properties of the system, TDDFT shows ways to look into excited state properties and provides response functions. These exact theories, which use the density as

the basic variable, only lack perfection because the exchange correlation functional is not known. A work similar to the one in this thesis has already been done in [4–6] where different species of a transition metal were placed inside a silicon cage. In [4] TDDFT has been used to produce both optical-absorption and spin-susceptibility spectra of the silicon cages in an attempt to identify each cage.

This thesis is divided in five parts. In part II: Theory, the Many Body problem is presented in chapter 1, chapter 2 reviews Density Functional Theory and chapter 3 introduces Time-Dependent Density Functional theory. In part III: Numerical Aspects, the Pseudopotential Approximation is shown, in chapter 4, while the Projector Augmented Wave method is discussed in chapter 5. Besides, part IV: Applications contains the Methodology used in this work in chapter 6 and the results obtained are gathered in chapters 7 and 8: Silicon cages with one transition metal atom and Silicon cages with two transition metal atoms, respectively. Finally in part V, some conclusions and future work are presented.

Part II

Theory

Chapter 1

The Many Body Problem

There are **mysteries** which men can only guess at, which age by age they may solve only in part.

Bram Stoker

1.1 A look into Many-Body theory

Mysteries... The Many-Body problem [7, 8] shows perfectly how both complicated and unrewarding physics can be. Think of an atom, or a molecule, placed in any region of space and time, subject to whichever field, or fields, and basically try to name all the interactions that maintain its structure and keep the electrons bound to the nuclei, or not, if the field is strong enough... Now disregard almost all of them, except for the interactions between electrons and nuclei and their self interactions. Oh, and electrons and nuclei can move, but not very fast. One should try to avoid those relativistic shenanigans as much as possible. This is the many-body problem. Now, try to solve it. The peculiarity of this problem is that, even after so much simplifications, it remains rather unsolvable... Strangely this is what motivates physicists the most. The joy of the challenge, that dwell within every phenomena exhibited by matter. Not only that, but the elegance of nature, hidden behind the mysteries of the universe, and unveiled by that undoubtedly extraordinary approach. It is quite remarkable.

Also, further clarification should be made, about something that may, or may not, have been written somewhere, relativity is awesome! And indispensable.

1.2 Interactions of electrons and nuclei

The Hamiltonian for a system of N electrons and M nuclei can be written as

$$\begin{aligned}\hat{H}(\mathbf{r}_1,...,\mathbf{r}_N,\mathbf{R}_1,...,\mathbf{R}_M) \;=\; & -\frac{1}{2}\sum_{i=1}^{\mathrm{N}}\nabla_i^2 \;-\; \sum_{i,I=1}^{\mathrm{N,M}}\frac{Z_I}{|\mathbf{r}_i-\mathbf{R}_I|} \;+ \\ & +\frac{1}{2}\sum_{\substack{i,j=1\\ i\neq j}}^{N}\frac{1}{|\mathbf{r}_i-\mathbf{r}_j|} - \sum_{I=1}^{\mathrm{M}}\frac{1}{2m_I}\nabla_I^2 \;+\; \frac{1}{2}\sum_{\substack{I,J=1\\ I\neq J}}^{\mathrm{M}}\frac{Z_I Z_J}{|\mathbf{R}_I-\mathbf{R}_J|},\end{aligned} \tag{1.1}$$

where the lower case subscripts denote electrons at position $\mathbf{r}_i$ and the upper case subscripts denote nuclei at position $\mathbf{R}_I$. Here and throughout this thesis Hartree atomic units are use. These units arise from casting the Schrödinger equation in a dimensionless form as well as defining

$$e = m_e = \hbar = 4\pi\epsilon_0 = 1. \tag{1.2}$$

In the last equation e stands for electron charge, m_e for electron mass, $\hbar$ for the Planck's constant and ϵ_0 for the electric permeability of vacuum. In this unit system length is given in bohr (1 $\mathrm{a_0} = \frac{4\pi\epsilon_0\hbar}{m_e e^2} = 0.5292$ Å), and energy in hartree (1 Ha $= \frac{e^2}{4\pi\epsilon_0 a_0} = 27.211$ eV), the speed of light is $c \simeq 137$, the unit of time is $\frac{\hbar}{\mathrm{Ha}} = 2.419\times10^{-17}\ s$, and the unit of force is $\frac{\mathrm{Ha}}{\mathrm{a_0}} = 8.24\times10^{-8}$ N.
The first term of the aforementioned Hamiltonian is the kinetic energy operator for electrons,

$$\hat{T} \;=\; -\frac{1}{2}\sum_{i=1}^{N}\nabla_i^2, \tag{1.3}$$

while the second term, the potential operator, represents the interaction between

electrons and nuclei,

$$\hat{V} \;=\; \sum_{i,I=1}^{\mathrm{N,M}} v(\mathbf{r}_i, \mathbf{R}_I), = - \sum_{i,I=1}^{\mathrm{N,M}} \frac{Z_I}{|\mathbf{r}_i - \mathbf{R}_I|}, \tag{1.4}$$

and the third, is the electron-electron interaction operator,

$$\hat{W} \;=\; \frac{1}{2} \sum_{i \neq j}^{N} \frac{1}{|\mathbf{r}_i - \mathbf{r}_j|}. \tag{1.5}$$

The last two terms are the nuclei kinetic operator and the nuclei-nuclei interaction operator

$$\hat{T}_{\mathrm{N}} \;=\; -\frac{1}{2m_I} \sum_{I=1}^{M} \nabla_I^2 \,, \qquad \hat{W}_{\mathrm{N}} \;=\; \frac{1}{2} \sum_{I \neq J}^{M} \frac{1}{|\mathbf{R}_I - \mathbf{R}_J|}. \tag{1.6}$$

1.2.1 Schrödinger equation

The fundamental equation governing a non-relativistic quantum system is the time dependent Schrödinger equation,

$$\mathrm{i} \frac{\partial}{\partial t} \Psi(\{\mathbf{r}\}, \{\mathbf{R}\}, t) \;=\; \hat{H}(\{\mathbf{r}\}, \{\mathbf{R}\}) \Psi(\{\mathbf{r}\}, \{\mathbf{R}\}, t). \tag{1.7}$$

The abbreviation $\{\mathbf{r}\} = (\mathbf{r}_1, ..., \mathbf{r}_N)$ was used, as well as $\mathbf{r}_i \equiv (\mathbf{r}_i', \sigma_i)$, that is the many-body wavefunction is a function of $3(N+M)$ spacial coordinates and $N+M$ spin coordinates.
As the Hamiltonian (1.1) is time-independent, the eigenstates of (1.7) can be written as $\Psi(\{\mathbf{r}\}, \{\mathbf{R}\}, t) = \Psi(\{\mathbf{r}\}, \{\mathbf{R}\}) e^{-\mathrm{i}Et}$, where $\Psi(\{\mathbf{r}\}, \{\mathbf{R}\})$ is the solution of the time-independent Schrödinger equation,

$$\hat{H}(\{\mathbf{r}\}, \{\mathbf{R}\}) \Psi(\{\mathbf{r}\}, \{\mathbf{R}\}) = E \Psi(\{\mathbf{r}\}, \{\mathbf{R}\}). \tag{1.8}$$

Alas, this equation is normally impossible to solve.

1.2.2 Born-Oppenheimer Approximation

Inspection of the many-body Hamiltonian provides a clue towards the simplification of the many-body problem: the only small parameter is the inverse nuclear mass, i.e. the nuclear kinetic energy term. As the electrons' mass is smaller than the mass of the nuclei, when the nuclei move, the electrons appear to adjust their positions instantaneously. Therefore, the electrons move adiabatically with the nuclei. This motivates the description of each nuclei as a point like static charge and is the reasoning behind the adiabatic or Born-Oppenheimer approximation [3, 7, 9]. Let the eigenvalues and the eigenfunctions for the electrons $E_i(\mathbf{R})$ and $\Psi_i(\{\mathbf{r}\} : \{\mathbf{R}\})$, which depend upon the nuclear positions as parameters, be the solution of

$$\hat{H}'(\{\mathbf{r}\}, \{\mathbf{R}\})\Psi_i(\{\mathbf{r}\} : \{\mathbf{R}\}) = E_i\Psi_i(\{\mathbf{r}\} : \{\mathbf{R}\}), \tag{1.9}$$

where the electron Hamiltonian is given by

$$\hat{H}'(\{\mathbf{r}\}, \{\mathbf{R}\}) \;=\; \{\hat{T} + \hat{W} + \hat{V}\}. \tag{1.10}$$

As electrons obey Pauli's exclusion Principle, this electron, many-body, wavefunction $\Psi_i(\{\mathbf{r}\} : \{\mathbf{R}\})$ must be antisymmetric with respect to the interchange of any two electrons. Let $\hat{P}_{ij}$ be an exchange operator that permutes the coordinates of the electrons i and j:

$$\hat{P}_{ij}\Psi_i(\mathbf{r}_1, ..., \mathbf{r}_i, ..., \mathbf{r}_j, ...\mathbf{r}_N : \{\mathbf{R}\}) = -\Psi_i(\mathbf{r}_1, ..., \mathbf{r}_j, ..., \mathbf{r}_i, ...\mathbf{r}_N : \{\mathbf{R}\}). \tag{1.11}$$

Since the electrons are indistinguishable, the new wavefunction and any other wavefunctions created by application of the exchange operator are also eigenfunctions of the Hamiltonian (1.10).
The full solution for the coupled system (1.8) can be written in terms of $\Psi_i(\{\mathbf{r}\} : \{\mathbf{R}\})$ because this wavefunction defines a complete set of states for the electrons at each $\{\mathbf{R}\}$. Therefore,

$$\Psi(\{\mathbf{r}\}, \{\mathbf{R}\}) = \sum_i \xi_i(\{\mathbf{R}\})\Psi_i(\{\mathbf{r}\} : \{\mathbf{R}\}). \tag{1.12}$$

In the pursuit of decoupled equations for electrons and nuclei, one has to insert the previous expansion in (1.8), multiply the expression on the left by $\Psi_i^\dagger(\{\mathbf{r}\} : \{\mathbf{R}\})$ and integrate over the electron variables in order to obtain the equations for $\xi_i(\{\mathbf{R}\})$:

$$\left[\hat{T}_\mathrm{N} + \hat{W}_\mathrm{N}(\{\mathbf{R}\}) + E_i(\{\mathbf{R}\})\right]\xi_i(\{\mathbf{R}\}) + \sum_i C_{ii'}(\{\mathbf{R}\})\xi_i(\{\mathbf{R}\}) = E\xi_i(\{\mathbf{R}\}), \quad (1.13)$$

with $C_{ii'}(\{\mathbf{R}\}) = \left[A_{ii'}(\{\mathbf{R}\}) + B_{ii'}(\{\mathbf{R}\})\right]$ and

$$\begin{aligned} A_{ii'}(\{\mathbf{R}\}) &= \sum_J \frac{1}{m_J} \int d^3\{r\}\Psi_i^\dagger(\{\mathbf{r}\} : \{\mathbf{R}\})\nabla_J\Psi_{i'}(\{\mathbf{r}\} : \{\mathbf{R}\})\nabla_J, \\ B_{ii'}(\{\mathbf{R}\}) &= \sum_J \frac{1}{2m_J} \int d^3\{r\}\Psi_i^\dagger(\{\mathbf{r}\} : \{\mathbf{R}\})\nabla_J^2\Psi_{i'}(\{\mathbf{r}\} : \{\mathbf{R}\}). \end{aligned} \quad (1.14)$$

At last, the only thing left in order to decouple the equations are the off-diagonal terms $C_{ii'}$, since $A_{ii}(\{\mathbf{R}\}) = 0$ from the normalization condition, whereas $B_{ii}(\{\mathbf{R}\})$ can be added to $\hat{W}_\mathrm{N}(\{\mathbf{R}\})$ to determine a modified potential function for the nuclei $\hat{U}_i(\{\mathbf{R}\}) = \hat{W}_\mathrm{N}(\{\mathbf{R}\} + B_{ii}(\{\mathbf{R}\})$. The Born-Oppenheimer approximation consists in neglecting those terms, i.e., the electrons are assumed to remain in a given state k as the nuclei move. Although the electron wave function and the energy of the state k change, no energy is transferred between the nuclear degrees of freedom and the excitations of the electrons. This approximation is rather good and only presents problems when degeneracies of the electronic states make the off-diagonal terms become large. Thus, the decoupled equations can be written as

$$\begin{aligned} \{\hat{T} + \hat{W} + \hat{V}\}(\{\mathbf{r}\}, \{\mathbf{R}\})\Psi_i(\{\mathbf{r}\} : \{\mathbf{R}\}) &= E_i\ \Psi_i(\{\mathbf{r}\} : \{\mathbf{R}\}) \\ \{\hat{T}_\mathrm{N} + \hat{U}_i(\{\mathbf{R}\}) + E_i(\{\mathbf{R}\})\}\ \xi_i(\{\mathbf{R}\}) &= E\ \xi_i(\{\mathbf{R}\}). \end{aligned} \quad (1.15)$$

In spite of the simplifications that arose from the adiabatic approximation, these equations are far too difficult to solve for a reasonable number of electrons and nuclei. Normally, in electronic structure, the equation for the nuclei is neglected in favour of a classical one while the equation for the electrons is further simplified.

From this point forward, the dependency of the electron wavefunctions with the nuclear coordinate will be omitted from the equations for simplicity.

1.3 The Rayleigh-Ritz principle

Before attempting to solve the first equation of (2.2), it is important to understand the Variational or Rayleigh-Ritz principle [10].
The average of many measurements of the energy of a system in state Ψ can be written as a functional of that state:

$$E[\Psi] = \frac{\langle\Psi|\,\hat{H}\,|\Psi\rangle}{\langle\Psi|\Psi\rangle}. \tag{1.16}$$

Furthermore, since each measurement of the energy provides one of the eigenvalues of $\hat{H}$, the energy calculated from a guess Ψ has to be an upper bound to the ground state energy E_0

$$E_0 \leq E[\Psi]. \tag{1.17}$$

This can be easily proven by insertion of $\Psi = \sum_i C_i\Psi_i$ in the energy functional

$$E[\Psi] = \frac{\sum_i |C_i|^2 E_i}{\sum_i |C_i|^2}. \tag{1.18}$$

As $E_0 \leq E_1 \leq E_2 \leq ...$, the minimum of the energy functional is only reached when $\Psi = C_0\Psi_0$.
Therefore, the ground state energy can be found by minimization of the energy functional with respect to all allowed N electron wave functions

$$E_0 \;=\; E[\Psi_0] \;=\; \min_{\Psi} E[\Psi]. \tag{1.19}$$

Consequently, the variation of the energy functional with respect to the wave function has to be stationary for the ground state, that is

$$\frac{\delta E[\Psi_0]}{\delta\Psi_0^*} \;=\; \frac{\hat{H}\Psi_0}{\langle\Psi_0|\Psi_0\rangle} - \frac{\langle\Psi_0|\,\hat{H}\,|\Psi_0\rangle\,\Psi_0}{\langle\Psi_0|\Psi_0\rangle^2} = 0 \quad \text{hence} \quad \hat{H}\Psi_0 \;=\; E_0\Psi_0. \tag{1.20}$$

In fact, all eigenstates are stationary points, therefore the Schrödinger equation can be written as

$$\delta[\langle\Psi|\,\hat{H}\,|\Psi\rangle - E(\langle\Psi|\Psi\rangle - 1)] = 0, \tag{1.21}$$

where E is the Lagrange multiplier.

1.4 Hellmann-Feynman Theorem

In classical mechanics, given a Hamiltonian $\hat{H}_{\mathbf{R}_I}$ depending on the parameter $\mathbf{R}_I$, one can define a force $F = -\frac{\partial \hat{H}}{\partial \mathbf{R}_I}$ which is associated with the parameter in the sense that $F\, d\mathbf{R}_I$ is the work done in changing the parameter by $d\mathbf{R}_I$. In Quantum Mechanics there are, in principle, two ways of calculating said force: $F = -\frac{\partial E_i}{\partial \mathbf{R}_I}$, where $E_i(\mathbf{R}_I)$ are the eigenvalues of state Ψ_i, or as $F = -\langle\Psi_i|\,\frac{\partial \hat{H}}{\partial \mathbf{R}_I}\,|\Psi_i\rangle$. The Hellmann-Feynman theorem ensures that both definitions are equivalent [11].
Derivation of the energy functional with respect to the nuclear coordinates, and assuming $\langle\Psi|\Psi\rangle = 1$ for convenience, leads to

$$\frac{\partial E}{\partial \mathbf{R}_I} \;=\; \langle\Psi|\,\frac{\partial \hat{H}}{\partial \mathbf{R}_I}\,|\Psi\rangle \;+\; \langle\frac{\partial \Psi}{\partial \mathbf{R}_I}|\hat{H}|\Psi\rangle \;+\; \langle\Psi|\hat{H}|\frac{\partial \Psi}{\partial \mathbf{R}_I}\rangle\,. \tag{1.22}$$

If the Hamiltonian is an Hermitian Operator and has eigenvalues E_i

$$\frac{\partial E}{\partial \mathbf{R}_I} \;=\; \langle\Psi|\,\frac{\partial \hat{H}}{\partial \mathbf{R}_I}\,|\Psi\rangle \;+\; \sum_i |C_i|^2 E_i \frac{\partial}{\partial \mathbf{R}_I}\,\langle\Psi_i|\Psi_i\rangle\,. \tag{1.23}$$

Then, conservative forces can be calculated as

$$F_{\mathbf{R}_I} = -\frac{\partial E}{\partial \mathbf{R}_I} \;=\; -\,\langle\Psi|\,\frac{\partial \hat{H}}{\partial \mathbf{R}_I}\,|\Psi\rangle \;=\; -\,\langle\Psi|\,\frac{\partial}{\partial \mathbf{R}_I}\big[\hat{V} + \hat{W}_N\big]\,|\Psi\rangle\,. \tag{1.24}$$

Chapter 2

Density Functional Theory

No great discovery was ever made without a bold **guess**.

Isaac Newton

2.1 A look into DFT

Guess... Currently, Density Functional Theory [10, 12, 13] provides the most popular methods used in electronic structure. This theory as become so widespread because it provides both accurate and swift results for many properties of atoms, solids and molecules. Simulations using DFT have discovered new materials and predicted many physical phenomena.

The success of this theory is related with the replacement of the wavefunction with the ground state density as the basic variable, therefore allowing to express all quantum mechanical observables as a functional of a real scalar function of three variables. This may not look like a big deal, but the storage space needed, when performing calculations with the wavefunction as the basic variable, scales with M^{3N}, where n is the number of electrons, the 3 accounts for the spacial coordinates and M for the mesh points (neglecting spin).

Another outstanding guess, partially responsible for the triumph of DFT was the replacement of a problem of interacting electrons by the problem of non-interacting particles under a peculiar potential.

2.2 Hohenberg-Kohn Theorems

The approach of Hohenberg-Kohn [14] consists in the formulation of Density Functional Theory as an exact theory of many body systems. The foundations of DFT consists in two theorems named after Hohenberg and Kohn.

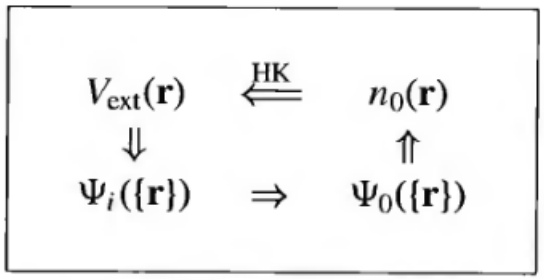

FIGURE 2.1: Schematic representation of the Hohenberg-Kohn Theorem. Starting with the potential and going down, the solution of the Schrödinger equation with the potential $\hat{V}_{\text{ext}}(\mathbf{r})$ determines all states of the system $\Psi_i(\{\mathbf{r}\})$, including the state with lesser energy, the ground state $\Psi_0(\{\mathbf{r}\})$ with density $n_0(\mathbf{r})$. The long arrow labelled HK connects the ground state density with the external potential.

The first of those theorems can be stated as:

Theorem 1 *The external potential $\hat{V}(\mathbf{r})$ of a system of interacting particles is a unique functional of the ground state density, apart from a trivial additive constant.*

The proof of this theorem starts by using the Schrödinger equation to obtain the non-degenerate ground state eigenfunctions and eigenvalues of equation (for the case of a degenerate ground state see [13])

$$\{\hat{T} + \hat{W} + \hat{V}\} |\Psi_0\rangle = \hat{H} |\Psi_0\rangle = E_0 |\Psi_0\rangle . \tag{2.1}$$

It is thus possible to define a surjective map between the set of external potentials and the ground state wavefunctions,

$$A : \ \{\hat{V}\} \longrightarrow \{\Psi_0\}. \tag{2.2}$$

Moreover, using the density operator

$$\hat{n} = \sum_{i}^{\mathrm{N}} \delta(\mathbf{r} - \mathbf{r}_i) \tag{2.3}$$

to calculate the ground state density

$$n(\mathbf{r}) = N \int d^3r \; d^3r_2 \; d^3r_3 \; ... \; d^3r_N |\Psi_0(\mathbf{r}_2, \mathbf{r}_3, ..., \mathbf{r}_N)|^2, \tag{2.4}$$

another surjective map is defined, now between the set of ground state wavefunctions and the ground state density:

$$B: \; \{\Psi_0\} \longrightarrow \{n_0\}. \tag{2.5}$$

The gist of the proof of the Hohenberg-Kohn theorem is that the maps A and B are also injective and thus bijective (fully invertible). That is, there is a one to one correspondence between the ground state electron density and the external potential:

$$\{\hat{V}\} \xleftarrow{A} \{\Psi_0\} \xleftarrow{B} \{n_0\}. \tag{2.6}$$

The demonstration that A is injective follows from *reductio ad absurdum*. One can speculate the existence of two external potentials, V and V' that differ by more than a constant and have the same ground state Ψ_0. In that case, from the difference of the Schrödinger equations

$$\{\hat{T} + \hat{W} + \hat{V}\} |\Psi_0\rangle = \hat{H} |\Psi_0\rangle = E_0 |\Psi_0\rangle , \tag{2.7}$$

$$\{\hat{T} + \hat{W} + \hat{V}'\} |\Psi_0\rangle = \hat{H}' |\Psi_0\rangle = E_0' |\Psi_0\rangle , \tag{2.8}$$

results

$$\{\hat{V} - \hat{V}'\} |\Psi_0\rangle = \{E_0 - E_0'\} |\Psi_0\rangle , \tag{2.9}$$

which clearly contradicts the assumption that the potentials differed by more than a constant.

On the other hand, the demonstration that B is injective also follows from *reductio ad absurdum*. Similarly to the last demonstration, let Ψ_0 and Ψ_0' be two different ground state solutions of the Schrödinger equation which originate the same ground state density. As A is bijective, two different ground state wavefunctions corresponds to two different external potentials (V and V'). Then, from the Rayleigh-Ritz variational principle,

$$E_0 = \langle \Psi_0 | \hat{H} | \Psi_0 \rangle < \langle \Psi_0' | \hat{H} | \Psi_0' \rangle , \tag{2.10}$$

$$E_0' = \langle \Psi_0' | \hat{H}' | \Psi_0' \rangle < \langle \Psi_0 | \hat{H}' | \Psi_0 \rangle , \tag{2.11}$$

which can be written as

$$E_0 < \langle \Psi_0' | \hat{H}' + \hat{V} - \hat{V}' | \Psi_0' \rangle = E_0' + \int d^3r [v(\mathbf{r}) - v'(\mathbf{r})] n_0(\mathbf{r}), \tag{2.12}$$

$$E_0' < \langle \Psi_0 | \hat{H} + \hat{V}' - \hat{V} | \Psi_0 \rangle = E_0 + \int d^3r [v'(\mathbf{r}) - v(\mathbf{r})] n_0(\mathbf{r}), \tag{2.13}$$

where (2.4) and $\hat{V} = \sum_i v(\mathbf{r}_i)$ as been used. Addition of both inequalities leads to the contradiction

$$E_0 + E_0' < E_0 + E_0'. \tag{2.14}$$

This establishes the desired result: there are no two external potentials which differ by more than a constant that originate the same ground state density. Therefore, the density uniquely determines the external potential (to within a constant).

Also, since the Hamiltonian is fully determined given the knowledge of the ground state density, the wavefunctions of all states are determined and, consequently, all properties of the system are completely determined.

Then, and because map B is invertible, that is $B^{-1} : \{n_0(\mathbf{r})\} \longrightarrow \{\Psi_0[n]\}$, the ground state expectation value of any observable $\hat{O}$ is a unique functional of the exact ground state density:

$$O[n_0] = \langle \Psi_0[n_0] | \hat{O} | \Psi_0[n_0] \rangle . \tag{2.15}$$

With this machinery at hand, one can dwell into the second Hohenberg-Kohn theorem:

Theorem 2 *For a particular external potential, a universal functional for the energy in terms of the density can be defined. Furthermore, the exact ground state energy of the system is the global minimum value of this functional and the minimizer density is the exact ground state density.*

This theorem establishes the variational character of the energy functional of the ground state density

$$\begin{aligned} E_v[n_0] &= \langle \Psi_0[n_0] | \hat{T} + \hat{W} + \hat{V} | \Psi_0[n_0] \rangle \\ &= T[n_0] + V_{\text{ee}}[n_0] + \int d^3r \; v(\mathbf{r}) n_0(\mathbf{r}) \\ &= F_{\text{HK}}[n_0] + \int d^3r \; v(\mathbf{r}) n_0(\mathbf{r}), \end{aligned} \tag{2.16}$$

where $\hat{V}$ is the external potential of a specific system with ground state density $n_0(\mathbf{r})$ and ground state energy E_0. The last equation also defines the universal functional F_{HK}. Universal because of the lack of dependence in $\hat{V}$, therefore this functional is the same for atoms, solids and molecules.

Application of the Rayleigh-Ritz variational principle results in

$$E_0 = E_v[n_0] = \langle \Psi_0[n_0] | \hat{H} | \Psi_0[n_0] \rangle \leq \langle \Psi[n] | \hat{H} | \Psi[n] \rangle = E_v[n]. \tag{2.17}$$

For that reason, a energy functional of the density can be defined

$$E_v[n] = \langle \Psi[n] | \hat{T} + \hat{W} + \hat{V} | \Psi[n] \rangle , \tag{2.18}$$

whose minimum is the ground state energy

$$E_0 = \min_n E_v[n]. \tag{2.19}$$

It is extraordinary that the ground state electron density uniquely determines the properties of the ground state, specially the ground state energy. Due to the close association between the electron density and the ground state in the Hohenberg-Kohn theorems, one can define a density to be *v-representable* if it is connected with the antisymmetric ground state wave function of a Hamiltonian with some external potential $v(\mathbf{r})$. The Hohenberg-Kohn theorems presented above are for *v-representable* densities. However, many reasonable densities have been shown to be non-*v-representable*.

Fortunately DFT can be formulated in a way that only requires the density to satisfy a weaker condition, the *N-representability* condition, which is satisfied by any reasonable density. A density is *N-representable* if it can be obtained from some antisymmetric wavefunction, which is a condition weaker than *v-representability*, since the later requires the former.

This formulation for *N-representable* densities is based on the Levy constrained-search [15] . Equation (1.19) shows that the ground state energy can be found by minimizing $\langle\Psi|\,\hat{H}\,|\Psi\rangle$ over all normalized, antisymmetric N-particle wavefunctions. However this minimization should be separated in two steps. First, a minimization over all wavefunctions Ψ which yield a given density $n(\mathbf{r})$:

$$E[n] = \min_{\Psi} \langle\Psi|\,\hat{H}\,|\Psi\rangle = \min_{\Psi} \langle\Psi|\,\hat{T} + \hat{W}\,|\Psi\rangle + \int d^3r\; v(\mathbf{r})n(\mathbf{r}), \tag{2.20}$$

since all wavefunctions that yield the same $n(\mathbf{r})$ also yield the same $\langle\Psi|\,\hat{W}\,|\Psi\rangle$. This also permits to define the universal functional

$$F[n] = \min_{\Psi} \langle\Psi|\,\hat{T} + \hat{W}\,|\Psi\rangle = T[n] + W[n], \tag{2.21}$$

which does not depend on the external potential, only on the density of electrons. Then the energy functional becomes

$$E[n] = F[n] + \int d^3r\; v(\mathbf{r})n(\mathbf{r}). \tag{2.22}$$

Finally, a minimization over all N-electron densities $n(\mathbf{r})$ with $v(\mathbf{r})$ constant, will yield the ground state density (which is the minimizing density)

$$E = \min_{\{n\}} E[n]. \tag{2.23}$$

This minimization should be taken with the restriction for the electron number. Formally this is achieved through the introduction of a Lagrange multiplier μ. Therefore, the variational equation is

$$\delta E = \delta\Big\{F[n] + \int d^3r\ v(\mathbf{r})n(\mathbf{r}) - \mu\ \Big(\int d^3r\ n(\mathbf{r})\ -\ N\Big)\Big\}\ =\ 0. \tag{2.24}$$

Carrying out the functional derivatives results in a Euler equation

$$\frac{\delta F[n]}{\delta n(\mathbf{r})} + v(\mathbf{r}) - \mu = \ 0. \tag{2.25}$$

Although the functional F[n] exists, as assured by the Hohenberg-Kohn Theorem, its exact form remains unknown until the resolution of the many-body problem for N electrons. So equation (2.25) can not be solved...

This could be a setback for DFT, as its purpose is an alternative way of solving the many-body problem resorting to the density instead of the wavefunction, and it would be, if not for the brilliant Kohn-Sham hypothesis.

2.3 Kohn-Sham Ansatz

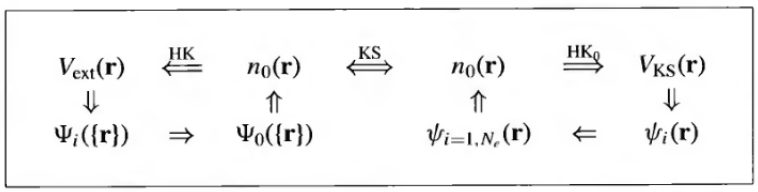

FIGURE 2.2: Schematic representation of the Kohn-Sham Ansatz. The left scheme shows the schematic representation of Hohenberg-Kohn theorem for interacting electrons while the right one shows the same but for non-interacting electrons. The ansatz connects both ground state densities.

Consider a system of N non-interacting electrons. In such a system the interaction operator $\hat{W}$ vanishes from the Hamiltonian. As the electrons behave in accordance to the Pauli Exclusion Principle, the ground state solution of a

system of N non-interacting electrons can be written as a Slater determinant of single-particle orbitals like

$$\psi(\mathbf{x_1}, \mathbf{x_2}..., \mathbf{x_N}) = \frac{1}{\sqrt{N}} \begin{bmatrix} \varphi_1(\mathbf{x_1}) & \varphi_2(\mathbf{x_1}) & \dots & \varphi_N(\mathbf{x_1}) \\ \varphi_1(\mathbf{x_2}) & \varphi_2(\mathbf{x_2}) & \dots & \varphi_N(\mathbf{x_2}) \\ \vdots & \vdots & \ddots & \vdots \\ \varphi_1(\mathbf{x_N}) & \varphi_2(\mathbf{x_N}) & \dots & \varphi_N(\mathbf{x_N}) \end{bmatrix},$$

where the orbitals that form the antisymmetric wavefunction satisfy the equation

$$\Big[-\frac{\nabla^2}{2} + v_\mathrm{s}[n](\mathbf{r}) \Big] \varphi_i(\mathbf{r}) = \epsilon_i \varphi_i(\mathbf{r}), \tag{2.26}$$

and the ground state density is given by

$$n(\mathbf{r}) = \sum_i^\mathrm{N} |\varphi_i(\mathbf{r}|^2. \tag{2.27}$$

The energy of this system can also be written as a functional of the density

$$E_\mathrm{s}[n] = T_\mathrm{s}[n] + \int d^3r \; v_\mathrm{s}(\mathbf{r}) n(\mathbf{r}), \tag{2.28}$$

and minimization of the aforementioned functional yields

$$\frac{\delta T_\mathrm{s}[n]}{\delta n(\mathbf{r})} + v_\mathrm{s}(\mathbf{r}) - \mu_\mathrm{s} = \; 0, \tag{2.29}$$

where μ_s is a different Lagrange multiplier than μ in (2.25). The approach of Kohn and Sham [16, 17] was to rearrange the terms in the energy functional of the interacting system

$$\begin{aligned} E[n] &= T[n] + W[n] + \int d^3r \; v(\mathbf{r}) n(\mathbf{r}) \\ &= T_\mathrm{s}[n] + (T[n] - T_\mathrm{s}[n]) + E_\mathrm{H}[n] + (W[n] - E_\mathrm{H}[n]) + \int d^3r \; v(\mathbf{r}) n(\mathbf{r}) \\ &= T_\mathrm{s}[n] + E_\mathrm{H}[n] + E_\mathrm{xc}[n] + \int d^3r \; v(\mathbf{r}) n(\mathbf{r}), \end{aligned} \tag{2.30}$$

where the Exchange-Correlation Energy Functional is defined as

$$E_{\mathrm{xc}}[n] = T[n] - T_{\mathrm{s}}[n] + W[n] - E_{\mathrm{H}}[n] \tag{2.31}$$

and the self-interaction energy of the density $n(\mathbf{r})$ treated as a classical charge density is defined as

$$E_{\mathrm{H}}[n] = \frac{1}{2}\int d^3r \int d^3r' \, \frac{n(\mathbf{r})n(\mathbf{r}')}{|\mathbf{r}-\mathbf{r}'|}. \tag{2.32}$$

Yet, the rearrangement in equation (2.30) can only be effectuated if one assumes that the ground state density of the interacting system can be represented as the ground state density of the non-interacting system. Thus, the Kohn-Sham hypothesis is that a system of non-interacting electrons exists, such that its density is the same of the interacting system. So, the Euler equation for the interacting system (2.25) now becomes

$$\frac{\delta T_{\mathrm{s}}[n]}{\delta n(\mathbf{r})} + v(\mathbf{r}) + v_{\mathrm{H}} + v_{\mathrm{xc}} - \mu = \ 0, \tag{2.33}$$

where the Hartree Potential is given by

$$v_{\mathrm{H}} = \frac{\delta E_{\mathrm{H}}[n]}{\delta n(\mathbf{r})} = \int d^3r' \, \frac{n(\mathbf{r}')}{|\mathbf{r}-\mathbf{r}'|}, \tag{2.34}$$

and the Exchange-Correlation potential by

$$v_{\mathrm{xc}} = \frac{\delta E_{\mathrm{xc}}[n]}{\delta n(\mathbf{r})}. \tag{2.35}$$

Equations (2.29) and (2.33) are equivalent if

$$\begin{aligned} v_{\mathrm{s}} &= v(\mathbf{r}) + v_{\mathrm{H}} + v_{\mathrm{xc}} - (\mu - \mu_{\mathrm{s}}) \\ &= v(\mathbf{r}) + v_{\mathrm{H}} + v_{\mathrm{xc}}. \end{aligned} \tag{2.36}$$

The difference between the Lagrange multipliers was added to v_{xc} in the last equation. So, assuming that the ground state density of the interacting system equals the ground state density of the non-interacting system, solving (2.33) is the same as solving (2.29) with the potential (2.36).

Therefore, for a given v_s, one obtains the density $n(\mathbf{r})$ that satisfies (2.33) by solving the N one-electron equations (2.26), since solving (2.29) is the same as solving (2.26). This yields the Kohn-Sham equations.

2.4 Kohn-Sham Equations and Eigenvalues

The Kohn-Sham equations can then be written as

$$\Big[-\frac{\nabla^2}{2} + v_{\mathrm{KS}}[n](\mathbf{r})\Big]\varphi_i(\mathbf{r}) = \epsilon_i\varphi_i(\mathbf{r}). \tag{2.37}$$

The Kohn-Sham equations describe non-interacting electrons that move subject to an effective potential, the Kohn-Sham potential, that has the form

$$v_{\mathrm{KS}}[n](\mathbf{r}) = v_{\mathrm{ext}}(\mathbf{r}) + v_{\mathrm{Hartree}}[n](\mathbf{r}) + v_{\mathrm{xc}}[n](\mathbf{r}). \tag{2.38}$$

Besides, one should expect no simple physical meaning for the Kohn-Sham wave-functions $\varphi_i(\mathbf{r})$ and eigenvalues ϵ_i. With the exception of the highest occupied eigenvalue, which is, approximately, minus the ionization potential I

$$\max_{occupied} \epsilon_i \simeq -I \tag{2.39}$$

there is none. Nevertheless, the density can be obtained from the Kohn-Sham wave functions as in equation (2.27).

Due to the functional dependence on the density, the Kohn-Sham equations form a set of non-linear coupled equations. The typical procedure to solve them is by iterating until self-consistency is achieved [12] (in a Self Consistent Field Cycle as depicted in figure 2.3). Normally, an initial density is supplied to start the iterative procedure.

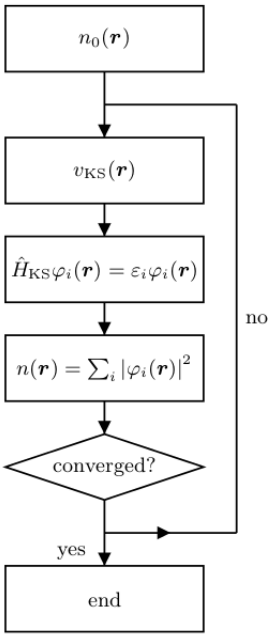

FIGURE 2.3: Flow chart depicting the Kohn-Sham SCF cycle.

Would the exact form of the exchange-correlation energy functional be known, solution of the Kohn-Sham equations should yield the exact ground state density and energy for the interacting system. Alas, the exact exchange correlation energy functional is not known and, therefore, has to be approximated.

2.4.1 Spin Density Form

The aforementioned Kohn-Sham equations are only valid in the spin-independent formalism. Regardless, DFT can be formulated within a spin-dependent formalism which account for external potentials with magnetic terms and spin dependences in the external potential or in the exchange-correlation functional (SDFT [18, 19]). Here is only presented the special case of a collinear spin polarized system with no external magnetic field applied and m_z will be referred to as the magnetization density because $\mathbf{m} = (0, 0, m_z)$) for a collinear spin system.

Let the ground state electron density and the magnetization density m_z have

the form

$$\begin{aligned} n(\mathbf{r}) &= n^{\uparrow}(\mathbf{r}) + n^{\downarrow}(\mathbf{r}) \\ m_z(\mathbf{r}) &= n^{\uparrow}(\mathbf{r}) - n^{\downarrow}(\mathbf{r}), \end{aligned} \tag{2.40}$$

where

$$n^{\sigma}(\mathbf{r}) = \sum_{i}^{\mathrm{N}} |\varphi_i^{\sigma}(\mathbf{r}|^2. \tag{2.41}$$

For this system, there are two sets of Kohn-Sham equations (one for spin up and another for spin down)

$$\Big[-\frac{\nabla^2}{2} + v_{\mathrm{ext}}^{\sigma}(\mathbf{r}) + v_{\mathrm{Hartree}}[n](\mathbf{r}) + v_{\mathrm{xc}}^{\sigma}[n, m_z](\mathbf{r}) \Big] \varphi_i^{\sigma}(\mathbf{r}) = \epsilon_i^{\sigma} \varphi_i^{\sigma}(\mathbf{r}). \tag{2.42}$$

Once again, with the Kohn-Sham equations in this form, collinear spin polarized systems can be described.

2.4.2 Relativistic Density Form

Sometimes relativistic effects are too important to be ignored and a relativistic extension of DFT has to be applied (RDFT [3, 20, 21]). With the assumption of collinearity, for the case where there is only an external scalar potential, no magnetic field and the system is not polarized, the Kohn-Sham equations can be extended to Dirac-like equations

$$\Big[\mathrm{i}c\boldsymbol{\alpha} \cdot \nabla + (\beta - 1)c^2 + v_{\mathrm{KS}}(\mathbf{r}) \Big] \varphi_i(\mathbf{r}) = \epsilon_i \varphi_i(\mathbf{r}), \tag{2.43}$$

where α and β are the usual Dirac matrices, v_{KS} is the usual Kohn-Sham potential, and the wavefunctions φ_i are four-component spinors. The density is evaluated as

$$n(\mathbf{r}) = \sum_{i} \varphi_i^{\dagger}(\mathbf{r}) \varphi_i(\mathbf{r}). \tag{2.44}$$

2.5 Exchange and Correlation Functionals

The exchange and correlation energy can be divided in two terms: the exchange energy and the correlation energy

$$E_{\mathrm{xc}}[n] = E_{\mathrm{x}}[n] + E_{\mathrm{c}}[n] = \int d^3r\ n(\mathbf{r})[\epsilon_x(n(\mathbf{r})) + \epsilon_c(n(\mathbf{r}))], \tag{2.45}$$

where $\epsilon_{xc} = \epsilon_x + \epsilon_c$ is the exchange correlation energy per particle of the system. The exchange energy can be related with the self-interaction correction (a classical effect which guarantees that an electron cannot interact with itself), and with the Pauli exclusion Principle, which tends to keep two electrons with parallel spin apart in space. While the correlation energy have connections to the Coulomb repulsion, which tends to keep any two electrons apart in space.

This energy functional has to be approximated as its correct form is unknown. The simplest approximation, and also the first is the local spin density approximation (LSDA, or only LDA for simplicity). Other example is the quite popular generalized gradient approximation (GGA).

2.5.1 Local Density Approximation

The LDA for the exchange-correlation energy was proposed in the original work of Kohn and Sham [16] and can be written as

$$E_{xc}^{\mathrm{LDA}}[n^{\uparrow}, n^{\downarrow}] = \int d^3r\ n(\mathbf{r})\epsilon_{xc}^{\mathrm{HEG}}(n^{\uparrow}(\mathbf{r}), n^{\downarrow}(\mathbf{r})), \tag{2.46}$$

where the exchange-correlation energy density of the system at a given point is equal to the exchange-correlation energy of the homogeneous electron gas. The exchange part is known analytically whereas the the correlation part is only known in the limits of high and low densities. Some points in between were generated by Monte-Carlo simulations [22]. Due to its relation to the homogeneous electron gas, it should work well only with fairly homogeneous systems. Surprisingly, it works well with inhomogeneous systems. It describes very well some physical properties of atoms, molecules and solids (like equilibrium geometries). But it also presents large errors (in eigenvalues per example).

2.5.2 Generalized gradient approximation

An improvement over LDA is the well known GGA. This approximation maintains correct physical features of the LDA and introduces a dependence on gradients of the density

$$E_{xc}^{\mathrm{GGA}}[n^{\uparrow}, n^{\downarrow}] = \int d^3r \; n(\mathbf{r})\epsilon_{xc}^{\mathrm{GGA}}(n^{\uparrow}(\mathbf{r}), n^{\downarrow}(\mathbf{r}), \nabla n^{\uparrow}(\mathbf{r}), \nabla n^{\downarrow}(\mathbf{r})). \tag{2.47}$$

To construct the exchange correlation energy functional one has to force the functional to obey some known physical constraints while avoiding problems with large gradients. While presenting good results for the energy calculations, most GGA, like the LDA, fail to reproduce the asymptotic behaviour of the exchange-correlation potential.

2.5.2.1 PBE

There are many examples of GGA functionals, like the GGA proposed by Perdew, Burk and Ernzerhof (PBE [23, 24]). The exchange part is given by

$$\begin{aligned} \epsilon_x^{\mathrm{PBE}} &= \epsilon_x^{\mathrm{HEG}} F_x^{\mathrm{PBE}} \\ F_x^{\mathrm{PBE}} &= 1 + k - \frac{k}{1 + (\mu s^2/k)}, \end{aligned} \tag{2.48}$$

where $k = 0.804$ and $\mu = 0.21951$. While the correlation part is chosen as

$$\epsilon_{xc}^{\mathrm{GGA}} = \epsilon_c^{\mathrm{HEG}} + H(r_s, \zeta, t), \tag{2.49}$$

where $(n^{\uparrow} - n^{\downarrow})/n$ is the spin polarization, r_s is the local value of the density parameter, and $t = |\nabla n|/(2\phi k_{TF} n)$ is a dimensionless gradient. Here $\phi = [(1+\zeta)^{2/3} + (1-\zeta)^{2/3}]/2$ and H is given by

$$H = \frac{e^2\gamma\phi^3}{a_0} \log\left(1 + \frac{\beta t^2}{\gamma} \frac{1 + At^2}{1 + At^2 + A^2t^4}\right). \tag{2.50}$$

The function A represents

$$A = \frac{\beta}{\gamma}\left[e^{\frac{-a_0\epsilon_c^{\mathrm{HEG}}}{e^2\gamma\phi^3}} - 1\right]^{-1}. \tag{2.51}$$

Chapter 3

Time Dependent Density Functional Theory

The only reason for **time** is so that everything doesn't happen at once.

Albert Einstein

3.1 A look into TDDFT

Time... TDDFT [25, 26] can be viewed as an exact reformulation of the time-dependent quantum mechanics, where the many body wave function is replaced in favor of the density. As DFT revolutionized electronic structure, by introducing the necessary machinery to obtain all the ground state properties of a system, TDDFT is proving to be a worthy extension both in name as in achievements. The methods to obtain the response of a system to an applied field, as propagation of the Kohn-Sham equations through time, have proven to be a remarkable way to study the excited states of a system, mainly for the possibilities they provide.

3.2 Runge-Gross Theorem

The time-dependent Schrödinger equation can be written as

$$\mathrm{i}\frac{\partial}{\partial t}\Psi(t) \;=\; \hat{H}(t)\Psi(t) = \;\{\hat{T}+\hat{W}+\hat{V}(t)\}\Psi(t), \tag{3.1}$$

where $\hat{T}$ and $\hat{W}$ are taken as in (1.3) and (1.5), and the time dependence of the Hamiltonian comes from a time dependent potential that may be expressed as

$$\hat{V}(t) \;=\; \sum_{i=1}^{N} v(\mathbf{r},t). \tag{3.2}$$

This potential includes the interaction between electrons and nuclei and an additional time-dependent term.

In order to formulate a proper Time-Dependent Density Functional Theory, one has to prove the Runge-Gross theorem [27], the time-dependent extension of the ordinary Hohenberg-Kohn theorem formulated in 1984.

Theorem 1 *For every potential $v(\mathbf{r},t)$ which can be expanded into a Taylor series with respect to the time coordinate around $t = t_0$, a map $G : v(\mathbf{r},t) \;\longrightarrow\; n(\mathbf{r},t)$ is defined by solving the time-dependent Schrödinger equation with a fixed initial state $\Psi(t_0) = \Psi_0$ and calculating the corresponding densities $n(\mathbf{r},t)$. This map can be inverted up to an additive merely time-dependent function in the potential.*

To prove this theorem, one has to show that two densities $n(\mathbf{r},t)$ and $n'(\mathbf{r},t)$ evolving from the same initial state Ψ_o through the influence of the potentials $v(\mathbf{r},t)$ and $v'(\mathbf{r},t)$, respectively, are always different by more than a time-dependent function

$$v(\mathbf{r},t) \;\neq\; v'(\mathbf{r},t) + c(t). \tag{3.3}$$

If this is true, the map G, defined as surjective in the theorem, is also injective

$$G : v(\mathbf{r},t) \;\longleftrightarrow\; n(\mathbf{r},t) \tag{3.4}$$

and can then be inverted. This one to one correspondence means that the time-dependent density determines the potential up to a purely time-dependent function and, therefore, the wavefunction is determined up to a purely time-dependent phase and can be expressed as a functional of the density and the initial state:

$$\Psi(t) \;=\; e^{\mathrm{i}\alpha(t)}\Psi[n,\Psi_0](t). \tag{3.5}$$

Consequently, the expectation value of any hermitian operator can also be revealed to be a functional of the density and the initial state

$$Q[n, \Psi_0](t) = \langle \Psi[n, \Psi_0](t)| \hat{O}(t) |\Psi[n, \Psi_0](t)\rangle \,. \tag{3.6}$$

The proof of the theorem can be divided in two steps. The first step consists in proving that different potentials, $v(\mathbf{r}, t)$ and $v'(\mathbf{r}, t)$, acting on the same initial state, originate different current densities $\mathbf{j}(\mathbf{r}, t)$ and $\mathbf{j}'(\mathbf{r}, t)$. The current density can be obtained from

$$\mathbf{j}(\mathbf{r}, t) = \langle \Psi(t)| \hat{\mathbf{j}} |\Psi(t)\rangle \,, \tag{3.7}$$

using the paramagnetic current density operator

$$\hat{\mathbf{j}}(\mathbf{r}) = \frac{1}{2i} \sum_{i=1}^{N} \Big[\nabla_i \delta(\mathbf{r} - \mathbf{r}_i) + \delta(\mathbf{r} - \mathbf{r}_i) \nabla_i \Big]. \tag{3.8}$$

As the initial state is the same for both primed and unprimed systems

$$\begin{aligned} \Psi(\mathbf{r}, t = 0) = \Psi'(\mathbf{r}, t = 0) = \Psi_0, \\ n(\mathbf{r}, t = 0) = n'(\mathbf{r}, t = 0) = n_0(\mathbf{r}), \\ \mathbf{j}(\mathbf{r}, t = 0) = \mathbf{j}'(\mathbf{r}, t = 0) = \mathbf{j}_0(\mathbf{r}), \end{aligned} \tag{3.9}$$

the application of the equation of motion for the expectation value of the current density,

$$\frac{\partial}{\partial t} \langle \Psi(t)| \hat{\mathbf{j}}(\mathbf{r}) |\Psi(t)\rangle = \langle \Psi(t)| \frac{\partial \hat{\mathbf{j}}}{\partial t} - \mathrm{i}[\hat{\mathbf{j}}(\mathbf{r}), \hat{H}(t)] |\Psi(t)\rangle \,, \tag{3.10}$$

yields

$$\begin{aligned} \frac{\partial}{\partial t}\mathbf{j}(\mathbf{r}, t) &= \frac{\partial}{\partial t} \langle \Psi(t)| \hat{\mathbf{j}}(\mathbf{r}) |\Psi(t)\rangle = -i \langle \Psi(t)| [\hat{\mathbf{j}}(\mathbf{r}), \hat{H}(t)] |\Psi(t)\rangle \\ \frac{\partial}{\partial t}\mathbf{j}'(\mathbf{r}, t) &= \frac{\partial}{\partial t} \langle \Psi'(t)| \hat{\mathbf{j}}(\mathbf{r}) |\Psi'(t)\rangle = -\mathrm{i} \langle \Psi'(t)| [\hat{\mathbf{j}}(\mathbf{r}), \hat{H}'(t)] |\Psi'(t)\rangle \,. \end{aligned} \tag{3.11}$$

Taking the difference of the last equations and evaluating it at the initial time

results in

$$\begin{aligned}\frac{\partial}{\partial t}\left[\mathbf{j}(\mathbf{r},t)-\mathbf{j}'(\mathbf{r},t)\right]_{t=0} &= -\mathrm{i}\left\langle\Psi_0\right|\left[\hat{\mathbf{j}}(\mathbf{r}),\hat{H}(0)-\hat{H}'(0)\right]\left|\Psi_0\right\rangle \\ &= -\mathrm{i}\left\langle\Psi_0\right|\left[\hat{\mathbf{j}}(\mathbf{r}),\hat{V}(0)-\hat{V}'(0)\right]\left|\Psi_0\right\rangle \\ &= -n_0(\mathbf{r})\nabla\left[v(\mathbf{r},0)-v'(\mathbf{r},0)\right].\end{aligned} \tag{3.12}$$

Now if $\left[v(\mathbf{r},0)-v'(\mathbf{r},0)\right]$ is different than a constant, the right hand side of (3.12) cannot vanish identically and the current densities will become different infinitesimally later than $t=0$. But this may not be true. Nevertheless, for potentials that can be expanded as a Taylor series with respect to the time coordinate around t = 0

$$v(\mathbf{r},t) = \sum_{k=0}^{\infty}\frac{t^k}{k!}\left[\frac{\partial^k}{\partial t^k}v(\mathbf{r},\mathbf{t})\right]_{t=0} \tag{3.13}$$

the condition (3.3) is equivalent to statement that there is a integer $k\geq 0$ such that

$$w_k(\mathbf{r}) = \frac{\partial^k}{\partial t^k}\left[v(\mathbf{r},t)-v'(\mathbf{r},t)\right]_{t=0}\neq 0. \tag{3.14}$$

So, application of the equation of motion $(k+1)$ times produces

$$\frac{\partial^{k+1}}{\partial t^{k+1}}\left[\mathbf{j}(\mathbf{r},t)-\mathbf{j}'(\mathbf{r},t)\right]_{t=0} = -n_0(\mathbf{r})\nabla w_k(\mathbf{r}) \neq 0. \tag{3.15}$$

Once more, infinitesimally later than the initial time,

$$\mathbf{j}(\mathbf{r},t) \neq \mathbf{j}'(\mathbf{r},t). \tag{3.16}$$

Therefore, this first step of the proof of the Runge-Gross theorem proves a one to one correspondence between potentials and current densities.

Similarly, the second step of the proof consists in proving that two different current densities imply two different densities. For that one uses the continuity equation,

$$\frac{\partial}{\partial t}n(\mathbf{r},t) = -\nabla\cdot\mathbf{j}(\mathbf{r},t), \tag{3.17}$$

to calculate the $(k+2)$ time-derivative of the both densities ($n(\mathbf{r},t)$ and $n'(\mathbf{r},t)$).

Taking the difference of the two at the initial time and using (3.14) results in

$$\frac{\partial^{k+2}}{\partial t^{k+2}}\big[n(\mathbf{r},t)-n'(\mathbf{r},t)\big]_{t=0} \;=\; \nabla\cdot\big[n_0(\mathbf{r})\nabla w_k(\mathbf{r})\big]. \tag{3.18}$$

Hence, if $\nabla\cdot\big[n_0(\mathbf{r})\nabla w_k(\mathbf{r})\big]\neq 0$, then the densities are different, which proves a one to one correspondence between the densities and the currents. To prove this, consider the integral

$$\begin{aligned}\int d^3r\; w_k(\mathbf{r})\nabla\cdot\big[n_0(\mathbf{r})\nabla w_k(\mathbf{r})\big] \;&=\; -\int d^3r\; n_0\big[\nabla w_k(\mathbf{r})\big]^2 \;+\\ &+\oint_S d\mathbf{S}\cdot\big[n_0(\mathbf{r})w_k(\mathbf{r})\nabla w_k(\mathbf{r})\big],\end{aligned} \tag{3.19}$$

where Green's theorem has been used. For potentials arising from normalizable external charge densities, the surface integral on the right vanishes. Besides, the remaining integrand on the right ($n_0\big[\nabla w_k(\mathbf{r})\big]^2$) is strictly positive (or zero if the density is also zero, which is not intended). As a consequence, the integrand on the left has to be different than zero. Then $\nabla\cdot\big[n_0(\mathbf{r})\nabla w_k(\mathbf{r})\big]$ cannot be zero everywhere and the proof of the Runge-Gross theorem is complete.

3.3 Time-Dependent Kohn-Sham Equations

Having established the Runge-Gross theorem, it is possible to construct a time-dependent Kohn-Sham scheme. First, one defines an auxiliary system of non-interacting electrons subjected to an external local potential v_{KS}. The Runge-Gross theorem states that this potential is unique and is chosen in a way that the density of the Kohn-Sham electrons is the same as the density of the original interacting system. Moreover, the Kohn-Sham electrons satisfy the time-dependent Scrödinger equation

$$\mathrm{i}\frac{\partial}{\partial t}\varphi_i(\mathbf{r},t)=\Big[-\frac{\nabla^2}{2}+v_{\mathrm{KS}}[n,\Psi_0,\Phi_0](\mathbf{r},t)\Big]\varphi_i(\mathbf{r},t), \tag{3.20}$$

whose orbitals provide the same density as the density of the interacting system:

$$n(\mathbf{r},t) \;=\; \langle\Phi(t)|\sum_i \delta(\mathbf{r}-\mathbf{r}_i)\,|\Phi(t)\rangle \;=\; \sum_i^{\mathrm{N}} |\varphi_i(\mathbf{r},t)|^2. \tag{3.21}$$

The time-dependent Kohn-Sham potential v_{KS} can be decomposed into:

$$v_{\mathrm{KS}}[n,\Psi_0,\Phi_0](\mathbf{r},t) = v_{\mathrm{ext}}[n,\Psi_0](\mathbf{r},t)+v_{\mathrm{Hartree}}[n](\mathbf{r},t)+v_{\mathrm{xc}}[n,\Psi_0,\Phi_0](\mathbf{r},t). \tag{3.22}$$

This means that the difference between the external potential, that generates the density $n(\mathbf{r},t)$ in an interacting system with initial state Ψ_0, and the one-body potential, that generates the same density in a non-interacting system with initial state Φ_0, is the xc potential added to the classical Hartree potential

$$v_{\mathrm{Hartree}}[n](\mathbf{r},t) = \int d^3r' \frac{n(\mathbf{r}',t)}{|\mathbf{r}-\mathbf{r}'|}. \tag{3.23}$$

The external potential in v_{KS} can be conveniently defined as

$$v_{\mathrm{ext}}[n,\Psi_0](\mathbf{r},t) \;=\; v_{\mathrm{ext0}}[n,\Psi_0](\mathbf{r}) + \theta(t-t_0)v_{\mathrm{per}}[n](\mathbf{r},t), \tag{3.24}$$

that is, at $t < t_0$ the system is at the ground state under the effect of a static potential whilst at $t \geq t_0$ a time-dependent potential is applied to the system.
In this construction, the xc potential includes all non-trivial many body effects and has an extremely complex functional dependence on the density. Quantum mechanics shows that minimization of the total energy yields the ground state of a system. However, as the energy is not a conserved quantity in a time-dependent system subject to a time-dependent external potential, there can be no variational principle on the basis of the total energy. Still, there is an analogous quantity to the ground state energy, the quantum mechanical action

$$\mathcal{A}[\Psi] = \int_{t_0}^{t_1} dt\, \langle\Psi(t)|\,\mathrm{i}\frac{\partial}{\partial t} - \hat{H}(t)\,|\Psi(t)\rangle\,, \tag{3.25}$$

where $\Psi(t)$ is a N-body function. Unfortunately, using this action to define the xc potential, as $v_{\mathrm{xc}}(\mathbf{r},t) = \frac{\delta\mathcal{A}}{\delta n(\mathbf{r},t)}$, results in causality and boundary conditions problems. These problems were solved by van Leeuwen [28] by using the Keldysh

formalism and by introducing a new action functional $\tilde{\mathcal{A}}$ for which the xc potential could be written as a variation of this new action without problems. Yet this new functional dependence on the density is still immensely complex.

3.4 Adiabatic Approximation for Functionals

As the DFT exchange-correlation energy functional, the TDDFT xc potential is also unknown. This functional depends on the time-dependent density, which means that, rigorously, $v_{\mathrm{xc}}[n](\mathbf{r},t)$ depends on the entire history of the density. There are few xc functionals that satisfy this computationally demanding condition. On the contrary, there is a plethora of ground state xc functionals available for DFT, as the result of more than 46 years of active research. The adiabatic approximation neglects the time-dependence condition while taking advantage of the existing ground state xc functionals.

The adiabatic time dependent xc potential takes the form

$$v_{\mathrm{xc}}[n](\mathbf{r},t) = \tilde{v}_{\mathrm{xc}}[n](\mathbf{r})|_{n=n(\mathbf{r},t)}, \tag{3.26}$$

for spin-independent TDDFT, and

$$v^{\sigma}_{\mathrm{xc}}[n^{\uparrow},n^{\downarrow}](\mathbf{r},t) = \tilde{v}^{\sigma}_{\mathrm{xc}}[n^{\uparrow},n^{\downarrow}](\mathbf{r})|_{n^{\sigma}=n^{\sigma}(\mathbf{r},t)}, \tag{3.27}$$

for the spin-dependent version of TDDFT [29]. This quite dramatic approximation is expected to work only in cases where the temporal dependence is small, that is, when the time-dependent system is locally close to equilibrium.

Regardless of its problems in describing the situations when the electrons get away from the nuclei, the adiabatic local density approximation (ALDA), which is the simplest approximation for the TDDFT xc functional, yields remarkably good excitation energies for many systems. The AGGA (adiabatic generalized gradient approximation) xc functional is expected to behave in a similar way, having the same problems which arise from an incorrect asymptotic behaviour (the potential do not decay as $-1/r$) while reasonably describing the true response of the system. Actually, both ALDA and AGGA provide similar excitation energies, as the KS orbital energy differences are reasonably good approximations to those energies

and the xc kernel only has to add a small correction on top of that estimate. In fact, simple approximations provides good results while similar approximations provide almost identical results.

3.5 Response Functions

In spectroscopic experiments, a sample is subjected to an external field $F(\mathbf{r}, t)$. Then, the sample, which is a fully interacting many-body system, responds to the field. This response can be measured by the change of some physical observable $\mathscr{P}$:

$$\Delta\mathscr{P} \;=\; \Delta\mathscr{P}_F[F]. \tag{3.28}$$

Clearly, as this functional has to reproduce the response for a field of any strength and shape, the dependence of the functional $\Delta\mathscr{P}_F$ on F is very complex. Nevertheless, for a weak field, the response can be expanded as a power series with respect to the field strength.

The first order response of an observable consists on a convolution of the linear response function $\chi^{(1)}_{\mathscr{P}\leftarrow F}$ with the variation of the field $\delta F^{(1)}$, expanded to the first order in the field strength.

$$\delta\mathscr{P}^{(1)}(\mathbf{r}, t) \;=\; \int dt' \int d^3r' \; \chi^{(1)}_{\mathscr{P}\leftarrow F}(\mathbf{r}, \mathbf{r}', t, t')\delta F^{(1)}(\mathbf{r}', t'), \tag{3.29}$$

where

$$\chi^{(1)}_{\mathscr{P}\leftarrow F}(\mathbf{r}, \mathbf{r}', t, t') \;=\; \left[\frac{\delta\mathscr{P}^{(1)}(\mathbf{r}, t)}{\delta F^{(1)}(\mathbf{r}', t')}\right]_{\delta F^{(1)}(\mathbf{r}', 0)}. \tag{3.30}$$

The linear response can also be cast in terms of the frequency ω in frequency space

$$\delta\mathscr{P}^{(1)}(\mathbf{r}, \omega) \;=\; \int d^3r' \; \chi^{(1)}_{\mathscr{P}\leftarrow F}(\mathbf{r}, \mathbf{r}', \omega)\delta F^{(1)}(\mathbf{r}', \omega). \tag{3.31}$$

On the other hand, second-order response can be written as

$$\begin{aligned}\delta\mathscr{P}^{(2)}(\mathbf{r},t) &= \frac{1}{2}\int dt' \int dt'' \int d^3r' \int d^3r'' \times \\ &\chi^{(2)}_{\mathscr{P}\leftarrow F}(\mathbf{r},\mathbf{r}',\mathbf{r}'',t,t',t'')\delta F^{(1)}(\mathbf{r}',t')\delta F^{(1)}(\mathbf{r}'',t'') \\ &+ \int dt' \int d^3r' \; \chi^{(1)}_{\mathscr{P}\leftarrow F}(\mathbf{r},\mathbf{r}',t-t')\delta F^{(2)}(\mathbf{r}',t').\end{aligned} \tag{3.32}$$

Higher-order responses have a similar straightforward construction withal.

3.5.1 Linear Response and Photo-absorption Spectra

One of the most important response functions is the linear density response function

$$\delta n(\mathbf{r},\omega) = \int d^3r' \; \chi_{n\leftarrow v_{per}}(\mathbf{r},\mathbf{r}',\omega)\delta v_{per}(\mathbf{r}',\omega), \tag{3.33}$$

which gives the linear response of the density to an external scalar perturbative potential $\delta v_{per}(\mathbf{r}',\omega)$. If the density response function $\chi_{n\leftarrow v_{per}}(\mathbf{r},\mathbf{r}',\omega)$ can be calculated, it can be used to obtain the first-order response of all properties derivable from the density with respect to any scalar field. An example is the polarizability α. Consider a finite system of electrons and nuclei which are subjected to an electrical field E. The response of the system to this electrical field is characterized by a variation of the time-dependent induced electrical dipole moment μ, which for finite systems can be expressed as a Taylor expansion [30]

$$\begin{aligned}\mu_i = \mu_{i0} + \sum_j \alpha_{ij}(\omega)E^{\omega}_j + \sum_{j,k}\frac{1}{2!}\beta_{ijk}(\omega)E^{\omega_1}_j E^{\omega_2}_k + \\ + \sum_{j,k,l}\frac{1}{3!}\gamma_{ijkl}(\omega)E^{\omega_1}_j E^{\omega_2}_k E^{\omega_3}_l + ...,\end{aligned} \tag{3.34}$$

where the indices refer to spatial coordinates, α is the linear polarizability, β and γ are hyperpolarizabilities, and in each term $\omega = \sum_m \omega_m$ (i.e. in the second term $\omega = \omega_1 + \omega_2$). For a weak field

$$\delta\boldsymbol{\mu}(\omega) \;=\; -\alpha(\omega)\mathbf{E}(\omega), \tag{3.35}$$

where $\boldsymbol{\mu}(\omega)$ is the induced dipole moment $\delta\boldsymbol{\mu}(t) = \boldsymbol{\mu}(t) - \boldsymbol{\mu}(0)$ in the frequency domain. However, the dipole moment can also be calculated as

$$\boldsymbol{\mu}(t) \;=\; -\sum_{i=1}^{N} \langle\varphi_i(t)|\,\mathbf{r}\,|\varphi_i(t)\rangle \;=\; -\int d^3r\;\mathbf{r}n(\mathbf{r},t). \tag{3.36}$$

Therefore, the polarizability is given by

$$\begin{aligned} \alpha_{ij}(\omega) \;&=\; \frac{1}{E_j(\omega)}\int d^3r\;x_i\;\delta n(\mathbf{r},\omega) \\ &=\; \frac{1}{E_j(\omega)}\int d^3r\;x_i\int d^3r'\;\chi_{n\leftarrow v_{per}}(\mathbf{r},\mathbf{r}',\omega)\delta v_{per}(\mathbf{r}',\omega), \end{aligned} \tag{3.37}$$

where x_i are the components of $\mathbf{r}$. Now, for a dipole electric field along the x_j direction one has $\delta v_{per}(\mathbf{r},t) \;=\; -x_j E_j(t)\delta(t)$. So, replacing the Fourier transform of this potential in the last equation yields

$$\alpha_{ij}(\omega) \;=\; -\int d^3r\int d^3r'\;x_i\;\chi_{n\leftarrow v_{per}}(\mathbf{r},\mathbf{r}',\omega)x'_j. \tag{3.38}$$

Moroever, the polarizability can be used to calculate the photo absorption cross-section

$$\sigma_{ij}(\omega) \;=\; \frac{4\pi\omega}{c}\Im\big\{\alpha_{ij}(\omega)\big\}. \tag{3.39}$$

from which one can then obtain the average orientational absorption coefficient A:

$$A \;=\frac{1}{3}\mathrm{Tr}\big[\sigma(\omega)\big] =\; \frac{4\pi\omega}{c}\Im\Big\{\frac{1}{3}\mathrm{Tr}\big[\alpha(\omega)\big]\Big\}. \tag{3.40}$$

The photo absorption spectrum can then be obtained by plotting the average absorption coefficient as a function of the energy.

The polarizabilities α, β and γ shown in (3.34) allude to the electrical spin-independent response of a system to an applied electrical field. Therefore they are known as density-density response functions. Nevertheless, if a perturbation and/or an observable are spin-dependent, one can define more general response

functions known as susceptibilities [3]. These susceptibilities can refer to density-density, spin-density, density-spin and spin-spin response functions. When the perturbation potential acts differently on collinear spin-up and spin-down electrons, the linear response density becomes:

$$\delta n^{\sigma}(\mathbf{r},\omega) \;=\; \sum_{\sigma'} \int d^3r' \; \chi^{\sigma\sigma'}_{n\leftarrow v_{per}}(\mathbf{r},\mathbf{r}',\omega)\delta v^{\sigma'}_{per}(\mathbf{r}',\omega). \tag{3.41}$$

This equation shows how to calculate the change in the density (δn) from a change in the external potential δv_{ext}. Based on the spin-up and spin-down electron density one can define the variations of the total electron density and of the magnetization density (once again, refers to m_z) as

$$\delta n(\mathbf{r},\omega) \;=\; \delta n_{\uparrow}(\mathbf{r},\omega) + \delta n_{\downarrow}(\mathbf{r},\omega) \tag{3.42}$$

$$\delta m(\mathbf{r},\omega) \;=\; \delta n_{\uparrow}(\mathbf{r},\omega) - \delta n_{\downarrow}(\mathbf{r},\omega). \tag{3.43}$$

Combination of the last equations with equation (3.41), taken in the form $\delta n^{\sigma}(\mathbf{r},\omega) = \sum_{\sigma'} F[\chi^{\sigma\sigma'}, \delta v^{\sigma'}]$ for simplicity, yields:

$$\begin{aligned} \delta n(\mathbf{r},\omega) \;&=\; F[\chi^{\uparrow\uparrow},\delta v^{\uparrow}] + F[\chi^{\uparrow\downarrow},\delta v^{\downarrow}] + F[\chi^{\downarrow\uparrow},\delta v^{\uparrow}] + F[\chi^{\downarrow\downarrow},\delta v^{\downarrow}] \\ \delta m(\mathbf{r},\omega) \;&=\; F[\chi^{\uparrow\uparrow},\delta v^{\uparrow}] + F[\chi^{\uparrow\downarrow},\delta v^{\downarrow}] - F[\chi^{\downarrow\uparrow},\delta v^{\uparrow}] - F[\chi^{\downarrow\downarrow},\delta v^{\downarrow}]. \end{aligned} \tag{3.44}$$

Let the perturbation potentials in the previous equation have the form

$$\delta v^{\sigma\ [n]}_{per}(\mathbf{r},\omega) \;=\; -x_j E_j(\omega), \tag{3.45}$$

for a spin-independent perturbation (indicated by $[n]$) and,

$$\delta v^{\sigma[m]}_{per}(\mathbf{r},\omega) \;=\; -x_j E_j(\omega)\sigma_z, \tag{3.46}$$

with $\sigma_z = 1, -1$ if $\sigma_z = \uparrow, \downarrow$ for a spin-dependent perturbation (indicated by $[m]$).

Inserting these potentials into (3.44) results in

$$\begin{aligned}
\delta n^{[n]}(\mathbf{r},\omega) &= -\big(F[\chi^{\uparrow\uparrow},x_jE_j]+F[\chi^{\uparrow\downarrow},x_jE_j]+F[\chi^{\downarrow\uparrow},x_jE_j]+F[\chi^{\downarrow\downarrow},x_jE_j]\big)\\
\delta m^{[n]}(\mathbf{r},\omega) &= -\big(F[\chi^{\uparrow\uparrow},x_jE_j]+F[\chi^{\uparrow\downarrow},x_jE_j]-F[\chi^{\downarrow\uparrow},x_jE_j]-F[\chi^{\downarrow\downarrow},x_jE_j]\big)\\
\delta n^{[m]}(\mathbf{r},\omega) &= -\big(F[\chi^{\uparrow\uparrow},x_jE_j]-F[\chi^{\uparrow\downarrow},x_jE_j]+F[\chi^{\downarrow\uparrow},x_jE_j]-F[\chi^{\downarrow\downarrow},x_jE_j]\big)\\
\delta m^{[m]}(\mathbf{r},\omega) &= -\big(F[\chi^{\uparrow\uparrow},x_jE_j]-F[\chi^{\uparrow\downarrow},x_jE_j]-F[\chi^{\downarrow\uparrow},x_jE_j]+F[\chi^{\downarrow\downarrow},x_jE_j]\big).
\end{aligned} \tag{3.47}$$

Using equations (3.35) and (3.36) for the dipole moment and similar equations for the spin-dipole moment (obtained by replacing the density by the magnetization density, the dipole moment by the spin-dipole moment and considering α as a first order susceptibility), one finds

$$\begin{aligned}
\alpha_{ij}^{[nn]} &= \alpha_{ij}^{\uparrow\uparrow}+\alpha_{ij}^{\uparrow\downarrow}+\alpha_{ij}^{\downarrow\uparrow}+\alpha_{ij}^{\downarrow\downarrow}\\
\alpha_{ij}^{[mn]} &= \alpha_{ij}^{\uparrow\uparrow}+\alpha_{ij}^{\uparrow\downarrow}-\alpha_{ij}^{\downarrow\uparrow}-\alpha_{ij}^{\downarrow\downarrow}\\
\alpha_{ij}^{[nm]} &= \alpha_{ij}^{\uparrow\uparrow}-\alpha_{ij}^{\uparrow\downarrow}+\alpha_{ij}^{\downarrow\uparrow}-\alpha_{ij}^{\downarrow\downarrow}\\
\alpha_{ij}^{[mm]} &= \alpha_{ij}^{\uparrow\uparrow}-\alpha_{ij}^{\uparrow\downarrow}-\alpha_{ij}^{\downarrow\uparrow}+\alpha_{ij}^{\downarrow\downarrow},
\end{aligned} \tag{3.48}$$

where

$$\alpha_{ij}^{\sigma\sigma'}(\omega) = -\int d^3r \int d^3r'\; x_i\; \chi^{\sigma\sigma'}(\mathbf{r},\mathbf{r}',\omega)x'_j. \tag{3.49}$$

The density-density first order susceptibility, $\alpha_{ij}^{[nn]}$, is the same as the polarizability of equation (3.38).

3.5.2 Kohn-Sham Linear Response

The linear response function χ in equation (3.41) is very hard to calculate. However, TDDFT provides a way to obtain it via the non-interacting Kohn-Sham system [31]. Variation of the Kohn-Sham potential (3.22) yields

$$\delta v_{\mathrm{KS}}^{\sigma}(\mathbf{r},\omega) = \delta v_{ext}^{\sigma}(\mathbf{r},\omega)+\int d^3r\;\frac{\delta n(\mathbf{r}',\omega)}{|(\mathbf{r}-(\mathbf{r}'|}+\sum_{\sigma'}\int d^3r'\; f_{\mathrm{xc}}^{\sigma\sigma'}(\mathbf{r},\mathbf{r}',\omega)\delta n(\mathbf{r}',\omega), \tag{3.50}$$

with δn as in (3.42) and where $f_{\mathrm{xc}}^{\sigma\sigma'}(\mathbf{r},\mathbf{r}',\omega)$ is the Fourier transform of the xc kernel

$$f_{\mathrm{xc}}^{\sigma\sigma'}(\mathbf{r},\mathbf{r}',t-t') \;=\; \frac{\delta v_{\mathrm{xc}}^{\sigma}[n_\uparrow,n_\downarrow](\mathbf{r}',t')}{\delta n^{\sigma'}(\mathbf{r}',t')}. \tag{3.51}$$

Besides, in the Kohn-Sham system, the variation of the density can be written as

$$\delta n^{\sigma}(\mathbf{r},\omega) \;=\; \sum_{\sigma'}\int d^3r'\; \chi_{\mathrm{KS}}^{\sigma\sigma'}(\mathbf{r},\mathbf{r}',\omega)\delta v_{\mathrm{KS}}^{\sigma'}(\mathbf{r}',\omega). \tag{3.52}$$

The response function in the last equation, the density response function of the non-interacting electrons, may also be expressed in terms of the unperturbed stationary Kohn-Sham orbitals

$$\chi_{\mathrm{KS}}^{\sigma\sigma'}(\mathbf{r},\mathbf{r}',\omega) \;=\; \delta_{\sigma\sigma'}\sum_{jk}^{\infty}(f_{k\sigma}-f_{j\sigma})\frac{\varphi_{j\sigma}(\mathbf{r})\varphi_{j\sigma}^{*}(\mathbf{r}')\varphi_{k\sigma}(\mathbf{r}')\varphi_{k\sigma}^{*}(\mathbf{r})}{\omega-(\epsilon_{j\sigma}-\epsilon_{k\sigma})+\mathrm{i}\eta}. \tag{3.53}$$

Here η is a positive infinitesimal and, as usual, $\varphi_{j\sigma}$ and $\epsilon_{k\sigma}$ are the ground state Kohn-Sham orbitals and eigenvalues and $f_{j\sigma}$ indicates the occupation number. Combining equations (3.50) and (3.52) results in

$$\begin{aligned}\delta n^{\sigma}(\mathbf{r},\omega) \;=\; \sum_{\tau}\int d^3r'\chi_{\mathrm{KS}}^{\sigma\sigma'}(\mathbf{r},\mathbf{r}',\omega)\Bigg[\delta v_{\mathrm{ext}}^{\tau}(\mathbf{r}',\omega)+\int d^3x\frac{\delta n(x,\omega)}{|\mathbf{r}'-x|}+\\ +\sum_{\tau'}\int d^3x f_{\mathrm{xc}}^{\tau\tau'}(\mathbf{r},\mathbf{r}',\omega)\delta n^{\tau'}(\omega)\Bigg].\end{aligned} \tag{3.54}$$

Finally, inserting (3.41) and using the fact that v_{ext} is an arbitrary function, makes it possible to reveal the response function as a Dyson-like equation

$$\begin{aligned}\chi^{\sigma\sigma'}(\mathbf{r},\mathbf{r}',\omega) \;=\; \chi_{\mathrm{KS}}^{\sigma\sigma'}(\mathbf{r},\mathbf{r}',\omega)+\\ +\sum_{\tau\tau'}\int d^3x\int d^3x'\chi^{\sigma\tau}(\mathbf{r},\mathbf{r}',\omega)\left[\frac{1}{|x-x'|}+f_{\mathrm{xc}}^{\tau\tau'}(\mathbf{r},\mathbf{r}',\omega)\right]\chi_{\mathrm{KS}}^{\tau'\sigma'}(\mathbf{r},\mathbf{r}',\omega).\end{aligned} \tag{3.55}$$

If the exact functional $f_{\mathrm{xc}}[n^\uparrow,n^\downarrow]$ were known, a self-consistent solution of this

last equation would yield the exact response function of the interacting system. Of course, there are several approximations to the xc kernel yet, a full solution of (3.55) is still quite difficult numerically. Fortunately, there are several ways to circumvent this problem.

3.5.3 Time-Propagation Method

There are at least three ways to calculate response functions from TDDFT: the Sternheimer method, the Casida Method, and the time-propagation method.

In the Sternheimer method [32], which is a perturbative approach, solves for a specific order of the response for a specific field in frequency space. Higher-order responses can be calculated from the lower ones. While in the Casida Method [33], instead of discovering the response, one calculates the poles and residues of the first-order response function, which corresponds to finding the resonant transitions of a system. Finally, the time-propagation method [34] consists in explicitly propagating the system in time after the application of a perturbing potential to excite the ground-state. Afterwards the difference between the final and the initial dipole moment provides a response function.

Only the later method will be discussed here given its importance for this thesis (all response calculations were carried out using this method). First, one has to understand how a wavefunction is propagated. The Kohn-Sham equations and all other Schrödinger like equations may be rewritten in terms of its linear propagator $\hat{U}(t, t_0)$ as

$$\mathrm{i}\frac{\partial}{\partial t}\hat{U}(t, t_0) \;=\; \hat{H}_{\mathrm{KS}}(t)\hat{U}(t, t_0), \tag{3.56}$$

which has a solution in terms of the initial state $\varphi(\mathbf{r}, t_0)$

$$\varphi(\mathbf{r}, t) \;=\; \hat{U}(t, t_0)\varphi(\mathbf{r}, t_0). \tag{3.57}$$

The last differential equation can be integrated

$$\hat{U}(t', t) \;=\; \hat{1} - \mathrm{i}\int_t^{t'} d\tau\; \hat{H}_{\mathrm{KS}}(\tau)\hat{U}(\tau, t_0). \tag{3.58}$$

The evolution operator $\hat{U}(t',t)$ can be seen as a Dyson operator, therefore it can be rewritten as a Dyson's series

$$\hat{U}(t',t) \;=\; \hat{T}e^{-\mathrm{i}\int_t^{t'} d\tau\ \hat{H}_{\mathrm{KS}}(\tau)}. \tag{3.59}$$

Three properties of $\hat{U}(t',t)$ can be derived from its definition:

• For a Hermitian Hamiltonian, $\hat{U}(t',t)$ is unitary.

$$\hat{U}^{\dagger}(t+\Delta t,t) \;=\; \hat{U}^{-1}(t+\Delta t,t) \tag{3.60}$$

• $\hat{U}(t',t)$ has time reversal symmetry.

$$\hat{U}(t+\Delta t,t) \;=\; \hat{U}^{-1}(t,t+\Delta t) \tag{3.61}$$

•$\hat{U}(t_1,t_2) \;=\; \hat{U}(t_1,t_3)\hat{U}(t_3,t_2)$.
Therefore $\varphi(t)$ can be propagated in small time steps

$$\hat{U}(t+\Delta t,t) \;=\; \hat{T}e^{-\mathrm{i}\int_t^{t+\Delta t} d\tau\ \hat{H}_{\mathrm{KS}}(\tau)}. \tag{3.62}$$

Application of (3.62) is not trivial and to proceed further, one has to find an approximation for the full time-evolution operator, which are based on the approximation of the exponential of an operator. Luckily, there are several algorithms to approximate $e^{\hat{O(t)}}$, like polynomial expansions, Krylov subspace projection techniques and splitting schemes, and therefore, a handful of approximations for the time-dependent propagator, based on Magnus Expansions, the Exponential Midpoint Rule and splitting techniques (for more information one should check [25]).

An example of an approximation for $\hat{U}$, the enforced time-reversal symmetry method is presented: as in a time-reversible method, propagating backwards $\frac{\Delta t}{2}$ starting from $\varphi(t+\Delta t)$ or propagating forwards $\frac{\Delta t}{2}$ starting from $\varphi(t)$ should lead to the same result

$$e^{+\mathrm{i}\frac{\Delta t}{2}\hat{H}(t+\Delta t)}\varphi(t+\Delta t) \;= e^{-\mathrm{i}\frac{\Delta t}{2}\hat{H}(t)}\varphi(t). \tag{3.63}$$

Rearranging the terms provides the approximation for the propagator

$$\hat{U}_{ETRS}(t+\Delta t, t) \;=\; e^{-\mathrm{i}\frac{\Delta t}{2}\hat{H}(t+\Delta t)} e^{-\mathrm{i}\frac{\Delta t}{2}\hat{H}(t)}. \tag{3.64}$$

With this in mind, it is straightforward to understand the time-propagation method procedure. Let $\varphi_i(\mathbf{r}, 0)$, the solutions of the ground state Kohm-Sham equations, be the initial state for the system under study, and let $v_{\mathrm{per}}(t) = -x_j E_j \delta(t)$ be the form of the weak electric dipole spin-independent perturbation that excites the electrons of the initial state. Let also the Kohn- Sham Hamiltonian be written like $\hat{H}_{\mathrm{KS}}(t) \;=\; \hat{H}^0_{\mathrm{KS}}(t) + v_{\mathrm{per}}(t)$.

First, one needs to find $\varphi_i(\mathbf{r}, 0)$. The ground state is then perturbed at $t = 0$. The wavefunctions at $t = 0^+$ can be calculated using

$$\begin{aligned} \varphi_i(\mathbf{r}, 0^+) \;&= \hat{T} e^{-\mathrm{i}\int_0^{0^+} d\tau \, \left[\hat{H}^0_{\mathrm{KS}}(\tau) + v_{\mathrm{per}}(\tau)\right]} \varphi_i(\mathbf{r}, 0) \\ &= \hat{T} e^{-\mathrm{i}\int_0^{0^+} d\tau \, \left[\hat{H}^0_{\mathrm{KS}}(\tau) - x_j E_j \delta(\tau)\right]} \varphi_i(\mathbf{r}, 0) \\ &= e^{\mathrm{i} x_j E_j} \varphi_i(\mathbf{r}, 0). \end{aligned} \tag{3.65}$$

This phase-factor shifts the momentum of the electrons, giving them a coherent velocity field that causes the appearance of a polarization as the system evolves in time.

Finally, the system is propagated up to some finite time using recursively (3.62). Then the time-dependent dipole moment (3.36) can be used to extract the dynamic polarizability tensor

$$\alpha_{ij} \;=\; \frac{1}{K_j} \int_0^{\infty} dt \, \left[\mu_i(t) - \mu_i(0)\right] e^{-i\omega t} e^{-\eta t} + O(K_j), \tag{3.66}$$

where $e^{-i\omega t}$ comes from the Fourier transform and $e^{-\eta t}$ is a damping function attached because infinite time-propagation is not possible in practice. The photo-absorption Spectrum is obtained by calculating the average absorption coefficient as in (3.40) and plotting it as a function of the energy.

Part III

Numerical Aspects

Chapter 4

Pseudopotential Approximation

It always bothers me that according to the laws as we understand them today, it takes a **computing** machine an infinite number of logical operations to figure out what goes on in no matter how tiny a region of space and no matter how tiny a region of time ...

Richard Feynman

4.1 A look into Pseudopotentials

Computing... The nuclear attractive potential binds electrons to nuclei, those that are more bound are normally defined as inner core electrons while those that move more freely, and thus have a greater probability of binding with other atoms, are designated as valence electrons. In fact, binding properties are almost completely due to the valence electrons. Besides, near the nucleus, the valence electrons' wave functions oscillate rapidly due to the orthogonalization between wavefunctions. Actually, oscillations of the wave function can be translated into more kinetic energy to the electrons, which cancels the nucleus strong attractive potential and explains why the valence electrons move more freely and are lesser bound to the nuclei. Nevertheless, these oscillations hinder the electronic structure calculations, as computing becomes more demanding.

This motivates the pseudopotential approximation in which the strong Coulomb potential of the nucleus and the effects of the tightly bound core electrons are re-

placed by an effective (usually weaker) ionic potential acting on valence electrons, the pseudopotential.

Pseudopotentials have been presented in several creative ways in their long lasting history [12]. Starting with Fermi's effective interaction in scattering experiments, they evolved to empirical pseudo-potentials based on the Phillips and Kleinman cancelation idea, like the Ashcroft potential. With Topp and Hopfield suggestion, that the pseudopotentials should be adjusted in a way they accurately describe the valence charge density, the *ab-initio* pseudopotentials were born. Two examples of this family are the Norm-Conserving pseudopotentials of Hamann, Schlüter, and Chiang, described in this chapter, and the Vanderbilt's Ultra-Soft pseudopotentials, where the charge deficit resulting from the relaxation of the norm-conservation constraint is cancelled by a localized atom-centered augmentation charge.

The study of pseudopotentials has attracted so many people due to their importance to DFT. Pseudopotentials permit a much faster resolution of the Kohn-Sham equations while providing accurate results. Therefore, they are in part responsible for the wild sucess and quick proliferation of DFT.

4.2 Phillips and Kleinman Formal Construction

The Phillips and Kleinman Formal Construction of a Pseudopotential can be traced back to the orthogonalized plane wave method (OPW) [35], in which the valence wavefunctions $|\varphi_v\rangle$ were expanded in a plane wave basis orthogonal to the inner core states $|\varphi_c\rangle$. Let both groups of wavefunctions be the exact solutions of the Schrödinger equation with Hamiltonian $\hat{H}$. The valence wavefunctions can then be written as a sum of a smooth function (the pseudo wavefunction $|\tilde{\varphi}_v\rangle$) with an oscillating function related to the inner core wavefunctions:

$$|\varphi_v\rangle = |\tilde{\varphi}_v\rangle + \sum_c \alpha_{cv} |\varphi_c\rangle \,. \tag{4.1}$$

Application of $\langle\varphi_c|$ on the left side results in $\alpha_{cv} = -\langle\varphi_c|\tilde{\varphi}_v\rangle$. Therefore, the Schrödinger equation for the smooth orbital can be written as

$$\hat{H}\left|\tilde{\varphi}_v\right\rangle = E_v\left|\tilde{\varphi}_v\right\rangle + \sum_c (E_c - E_v)\left|\varphi_c\right\rangle\left\langle\varphi_c\right|\left|\tilde{\varphi}_v\right\rangle . \tag{4.2}$$

Thus, the pseudo wavefunctions satisfy a Schrödinger like equation, whose pseudo Hamiltonian $\hat{H}^{\mathrm{PK}}$ has an additional energy-dependent contribution

$$\hat{H}^{\mathrm{PK}}(E) = \hat{H} - \sum_c (E_c - E)\left|\varphi_c\right\rangle\left\langle\varphi_c\right| \tag{4.3}$$

or, after explicitly writing both Hamiltonians,

$$\hat{v}^{\mathrm{PK}}(E) = \hat{v} - \sum_c (E_c - E)\left|\varphi_c\right\rangle\left\langle\varphi_c\right| , \tag{4.4}$$

where $\hat{v}^{\mathrm{PK}}$ is the Phillips and Kleinman pseudopotential and $\hat{v}$ is the true potential. Outside the core region, $\hat{v}^{\mathrm{PK}}$ becomes equal to $\hat{v}$ due to the decay of the inner core states whereas, in the vicinity of the core, the pseudo potential becomes much weaker because of the additional repulsive contribution (the second term in (4.4)).

4.3 Norm-conserving Ab-Initio Pseudopotentials

When chasing for the perfect pseudopotential, there are two goals to have in mind: the pseudopotential should be as soft as possible and as transferable as possible. A soft pseudopotential means that pseudo wavefunctions can be expanded in less basis functions (like plane-waves), while transferability means that the pseudopotential can correctly describe different configurations, like crystals and molecules.

The quest for the perfect pseudopotential has lead to the norm-conserving pseudopotentials. In spite of existing better pseudopotentials by now, these norm-conserving pseudopotentials are widely used, partially for their simplicity and mainly for their capability at providing accurate results with reasonable speed.

Norm-conserving pseudopotentials are obtained through the following procedure [12] [36]:

1. Taking into account all electrons, the free atom radial Kohn-Sham equations

are solved, for a given configuration, in order to obtain the all electron wave functions.

As a Schrödinger like equation, the Kohn-Sham equation has a similar resolution. A spherical averaging of the density leads to a spherically symmetric Kohn-Sham potential. Then, a separation of variables in the wavefunction leads to the spherical harmonics and to the one-dimensional second-order equation

$$\Big[-\frac{1}{2}\frac{d^2}{dr^2} - \frac{1}{r}\frac{d}{dr} + \frac{l(l+1)}{2r^2} + v_{\mathrm{KS}}^{\mathrm{AE}}[n^{\mathrm{AE}}](r)\Big] R_{nl}^{\mathrm{AE}}(r) = \epsilon_{nl} R_{nl}^{\mathrm{AE}}(r), \qquad (4.5)$$

where

$$v_{\mathrm{KS}}^{\mathrm{AE}}[n^{\mathrm{AE}}](r) = -\frac{Z}{r} + v_{\mathrm{Hartree}}[n^{\mathrm{AE}}](r) + v_{\mathrm{xc}}[n^{\mathrm{AE}}](r). \qquad (4.6)$$

There are many methods to solve this equation, like the Shooting method.

2. Imposing the norm-conservation and other specific conditions, the pseudo wavefunctions are determined using a proper scheme. Denoting the core radius as r_{cl}, where l stands for the dependency of the core radius with the angular moment quantum number, these conditions can be written as

$$\begin{aligned} \epsilon_l^{\mathrm{PP}} &= \epsilon_{nl}^{\mathrm{AE}} \\ Q_l = \int_0^{r_{cl}} dr |R_l^{\mathrm{PP}}(r)|^2 r^2 &= \int_0^{r_{cl}} dr |R_{nl}^{\mathrm{AE}}(r)|^2 r^2, \quad \text{if} \\ R_l^{\mathrm{PP}}(r) &= R_{nl}^{\mathrm{AE}}(r) \quad \text{if } r > r_{cl}. \end{aligned} \qquad (4.7)$$

That is, the pseudo eigenvalues should match the true valence eigenvalues, the integrated charge inside the core radius for the wavefunction and for the pseudo wavefunction agrees and, the pseudo and the all electron wave function are equal beyond the core radius. Besides, the pseudo wavefunctions should not have nodal surfaces.

Two examples of schemes for the generation of the pseudopotential are

the Hamann Potential [37] and the Troulier-Martins Potential [38]. The latter scheme will be presented, as it was the one used to generate norm-conserving pseudopotentials in this thesis. In the Troulier-Martins scheme, the wave functions are defined as

$$R_l^{\mathrm{PP}}(r) = \begin{cases} R_{nl}^{\mathrm{AE}}(r), & \text{if } r > r_{cl} \\ r^l \mathrm{e}^{p(r)}, & \text{if } r \leq r_{cl}, \end{cases} \tag{4.8}$$

with

$$p(r) = \sum_i c_{2i} r^{2i} \qquad \text{with } i \in [0, 6]. \tag{4.9}$$

These coefficients are adjusted imposing the continuity of the pseudo wavefunctions and their derivatives until the fourth order at $r = r_{cl}$, norm conservation and that the screened pseudo potential has zero curvature at the origin.

Additionally, the Troullier-Martins Scheme can be extended in order to include semi core states into the valence space. This extension is known as multi-reference pseudopotentials and the difference for the normal Troullier-Martins scheme is three additional terms in (4.9). The new polynomial have to be adjusted using the same conditions as the ones used for the normal scheme applied to the semi-core pseudo wavefunctions and imposing the conditions (4.7) to the valence pseudo wavefunction.

3. Inversion of the radial Kohn-Sham equation for the pseudo wavefunction and the valence electron density results in the screened pseudopotential.

$$v_l^{\mathrm{PP,screened}}(r) = \epsilon_l^{\mathrm{PP}} - \frac{l(l+1)}{2r^2} + \frac{1}{2rR_l^{\mathrm{PP}}(r)} \frac{d^2}{dr^2}[rR_l^{\mathrm{PP}}(r)] \tag{4.10}$$

4. Finally, subtraction of the Hartree and exchange-correlation potentials yield the unscreened pseudopotential.

$$v^{\mathrm{PP}}(r) = v^{\mathrm{PP,screened}}(r) - v_{\mathrm{Hartree}}[n^{\mathrm{PP}}] - v_{xc}[n^{\mathrm{PP}}](r) \tag{4.11}$$

Chapter 5

The Projector Augmented Waves Method

Resistance is useless.

Doctor Who

5.1 A look into the PAW Method

Resistance... First introduced and implemented by Blöchl [39], the Projector Augmented Waves Method is an alternative to the pseudopotential approach. Since then it has been implemented in several codes, like ABINIT [40] and VASP [41, 42]. Although there was some resistance to use this method in the work presented in this thesis, this method proved to be faster and more efficient than methods based on norm-conserving pseudopotentials.

The PAW consists in dividing space in two regions: atom-centered augmentation spheres and an interstitial region. Throughout space, the wave function can be described by a pseudo wavefunction as in the pseudopotential approach. Nonetheless, within the augmentation region that description is a poor one. So, the idea behind the PAW method is to have all electron partial-waves functions inside those regions. Partial or atomic wave functions are only defined inside the augmentation region.

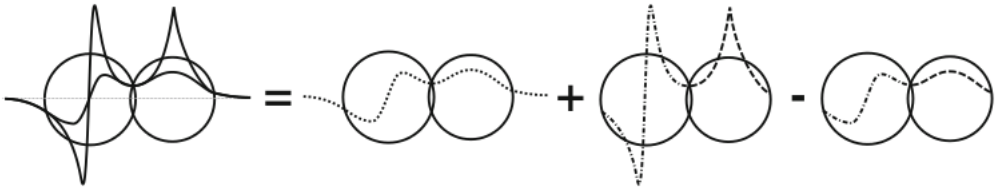

FIGURE 5.1: The All-electron PAW wavefunction as a sum of the pseudo wavefunction with the atomic partial wavefunction subtracted by the partial pseudo wavefunction.

The easiest way to do so, is to remove the pseudo wave function by subtracting a partial or atomic pseudo wavefunction while summing all electron atomic functions inside the augmentation region

$$|\varphi\rangle = |\tilde{\varphi}\rangle + \sum_i c_i(|\xi_i\rangle - |\tilde{\xi}_i\rangle). \tag{5.1}$$

This expression can be easily derived by expanding both the all electron and the pseudo wavefunctions in their respective partial-waves inside the augmentation sphere.

Obviously, for the wavefunction and its gradient to be continuous, an all electron partial-wave and its pseudo partial-wave must have the same logarithmic derivative at the boundary of the augmentation region.

Therefore, the PAW method precision and efficiency can already be explained: as the space is divided into two regions, so is the discretization of the functions. The smooth pseudo wavefunctions are evaluated on regular uniform grids and in contrast, the partial-waves are evaluated for each sphere individually on a radial grid. Consequently, one can have normal discretization in the interstitial region and a better one for the all electron functions inside each augmentation sphere.

5.2 Formalism

5.2.1 Transformation operator

In order to determine the transformation that changes the pseudo wavefunction to the wavefunction, one has to calculate the c_i coefficients of (5.1).

In the PAW method, this is done by defining the projectors $\tilde{p}_i$, which are localized inside augmentation spheres. These projectors are required to fulfill the condition that the one center expansion of a pseudo wavefunction is identical to itself, $\sum_i |\tilde{\xi}_i\rangle \langle \tilde{p}_i|\tilde{\varphi}_i\rangle = |\tilde{\varphi}_i\rangle$. Therefore, in the limit $\tilde{\xi}_i$ forms a complete sum:

$$\sum_i |\tilde{\xi}_i\rangle \langle \tilde{p}_i| = 1. \tag{5.2}$$

This implies that the projectors obey the orthonormality condition:

$$\langle \tilde{p}_i|\tilde{\xi}_j\rangle = \delta_{ij}. \tag{5.3}$$

Finally, applying these relations and some algebra tricks to (5.1) ,

$$\begin{aligned} |\varphi\rangle = (1 - \sum_i 1_i) |\tilde{\varphi}\rangle + \sum_i c_i(|\xi_i\rangle - |\tilde{\xi}_i\rangle) + \\ + \sum_i |\tilde{\xi}_i\rangle \langle \tilde{p}_i|\tilde{\varphi}_i\rangle \end{aligned} \tag{5.4}$$

results in

$$c_i = \langle \tilde{p}_i|\tilde{\varphi}_i\rangle . \tag{5.5}$$

Then, the transformation operator takes the form

$$\hat{\mathcal{T}} = \ 1 + \sum_i (|\xi_i\rangle - |\tilde{\xi}_i\rangle) \langle \tilde{p}_i| . \tag{5.6}$$

It can be used to write

$$|\varphi_j\rangle = \hat{\mathcal{T}} |\tilde{\varphi}_j\rangle \tag{5.7}$$

5.2.2 Operators

The PAW pseudo operators ($\tilde{O}$) can be obtained from the all-electron operators ($\hat{O}$) using (5.7):

$$\langle \varphi_i| \hat{O} |\varphi_j\rangle = \langle \tilde{\varphi}_i| \hat{\mathcal{T}}^\dagger \hat{O} \hat{\mathcal{T}} |\tilde{\varphi}_j\rangle = \langle \tilde{\varphi}_i| \tilde{O} |\tilde{\varphi}_j\rangle . \tag{5.8}$$

The form of the pseudo operator $\tilde{O} = \hat{\mathcal{T}}^{\dagger}\hat{O}\hat{\mathcal{T}}$ had to be evaluated both inside and outside the augmentation region Ω_R. Within the augmentation region, some terms will cancel as a consequence of (5.2) and

$$\tilde{O} = \sum_{ij} |\tilde{p}_i\rangle \langle\xi_i| \hat{O} |\xi_j\rangle \langle\tilde{p}_j| . \tag{5.9}$$

While outside the augmentation region the partial waves are equal $|\tilde{\xi}_i\rangle = |\xi_i\rangle$, so

$$\tilde{O} = \hat{O}. \tag{5.10}$$

Therefore, the pseudo operator can be written independently of the region of space where it is being evaluated as

$$\tilde{O} = \hat{\mathcal{T}}^{\dagger}\hat{O}\hat{\mathcal{T}} = \hat{O} + \sum_{ij} |\tilde{p}_i\rangle \left(\langle\xi_i| \hat{O} |\xi_j\rangle - \langle\tilde{\xi}_i| \hat{O} |\tilde{\xi}_j\rangle\right) \langle\tilde{p}_j| . \tag{5.11}$$

As an example, one can use the charge density operator and the later relation to calculate the PAW charge density as

$$n(\mathbf{r}) = \tilde{n}(\mathbf{r}) + n^1(\mathbf{r}) - \tilde{n}^1(\mathbf{r}), \tag{5.12}$$

where

$$\tilde{n}(\mathbf{r}) \;=\; \sum_i f_i \langle\tilde{\varphi}_i|\mathbf{r}\rangle \langle\mathbf{r}|\tilde{\varphi}_i\rangle \tag{5.13}$$

is the soft pseudo charge density and f_i is the occupation of the state. The charge densities calculated from the partial waves on a radial support grid can be defined as

$$n^1(\mathbf{r}) \;=\; \sum_{jk} \rho_{jk} \langle\xi_j|\mathbf{r}\rangle \langle\mathbf{r}|\xi_k\rangle , \tag{5.14}$$

$$\tilde{n}^1(\mathbf{r}) \;=\; \sum_{jk} \rho_{jk} \langle\tilde{\xi}_j|\mathbf{r}\rangle \langle\mathbf{r}|\tilde{\xi}_k\rangle , \tag{5.15}$$

with ρ_{jk} as the occupancies for each augmentation channel obtained from

$$\rho_{jk} = \sum_i f_i \langle \tilde{\varphi}_i | \tilde{p}_j \rangle \langle \tilde{p}_k | \tilde{\varphi}_i \rangle . \tag{5.16}$$

5.2.3 Total energy

The exact Kohn-Sham energy functional of the charge density is usually rewritten as

$$E = \sum_i f_i \langle \varphi_i | -\frac{\nabla^2}{2} | \varphi_i \rangle + E_{\mathrm{H}}[n + n_Z] + E_{\mathrm{xc}}[n] \tag{5.17}$$

when deriving the PAW energy functional. Here E_{xc} stands for the electronic exchange-correlation energy and E_{H} for the Hartree energy of the electronic charge density and the point charge density of the nuclei n_Z, which is present to account for the interaction between electrons and nuclei. As in the pseudopotential approach, the cores are taken to be frozen and the wavefunctions of the PAW method describe only the valence wave functions.

Before proceeding, there is a trick devised by Blöchl that consists in splitting the total charge terms in three terms to allow an efficient treatment of the long-range electrostatic interactions:

$$n + n_{Zc} = (\tilde{n} + \hat{n} + \tilde{n}_{Zc}) + (n^1 + n_{Zc}) - (\tilde{n}^1 + \hat{n} + \tilde{n}_{Zc}), \tag{5.18}$$

where n_{Zc} denotes the point charge density of the nuclei plus the frozen core all-electron charge density, whereas $\tilde{n}_{Zc}$ is the pseudized core density, which is equivalent to n_{Zc} outside the core radius and both have the same moment inside the core region.

Perhaps the most important part of equation (5.18), $\hat{n}$ represents a compensation charge that was introduced to cancel all multipole moments inside the augmentation sphere. The compensation charge is then added to the pseudo charge density to restore the cancelled multipoles. Alas, this term can be added because terms of the form $\hat{B} - \sum_{ij} |\tilde{p}_i\rangle \langle \tilde{\xi}_i | \hat{B} | \tilde{\xi}_j \rangle \langle \tilde{p}_j |$ can be added to the pseudo PAW operator without altering its expectation value.
Similar to the expectation values, the expression for the total energy can also be

divided as

$$E \;=\; \tilde{E} + E^1 - \tilde{E}^1 \tag{5.19}$$

into a smooth part $\tilde{E}$, which is evaluated on regular grids in Fourier (as a Fast Fourier transform grid) or real space, and two one-centre contributions E^1 and $\tilde{E}^1$ which are evaluated for each sphere individually on a radial support grids in an angular momentum representation. These parts are given by

$$\begin{aligned}\tilde{E} \;&=\; \sum_i f_i \,\langle\tilde{\varphi}_i| - \frac{\nabla^2}{2}\,|\tilde{\varphi}_i\rangle + E_{\mathrm{H}}[\tilde{n}+\hat{n}] + E_{\mathrm{xc}}[\tilde{n}+\hat{n}+\tilde{n}_c] + \\ &+ \int d^3\; v_{\mathrm{H}}[\tilde{n}_{Zc}]\{[\tilde{n}(\mathbf{r})+\hat{n}(\mathbf{r})\} + U(\mathbf{R}, Z_{ion}),\end{aligned} \tag{5.20}$$

$$\begin{aligned}E^1 \;&=\; \sum_{ij} \rho_{ij}\,\langle\xi_i| - \frac{\nabla^2}{2}\,|\xi_j\rangle + E_{\mathrm{H}}[n^1] + E_{\mathrm{xc}}[n^1+n_c] + \\ &+ \int_{\Omega_r} d^3\; v_{\mathrm{H}}[n_{Zc}]\{[n^1(\mathbf{r})+\hat{n}(\mathbf{r})\},\end{aligned} \tag{5.21}$$

$$\begin{aligned}\tilde{E}^1 \;&=\; \sum_{ij} \rho_{ij}\,\langle\tilde{\xi}_i| - \frac{\nabla^2}{2}\,|\tilde{\xi}_j\rangle + E_{\mathrm{H}}[\tilde{n}^1+\hat{n}] + E_{\mathrm{xc}}[\tilde{n}^1+\hat{n}+\tilde{n}_c] + \\ &+ \int_{\Omega_r} d^3\; v_{\mathrm{H}}[\tilde{n}_{Zc}]\{[\tilde{n}^1(\mathbf{r})+\hat{n}(\mathbf{r})\}.\end{aligned} \tag{5.22}$$

5.3 PAW Method practical scheme

5.3.1 Overlap Operator

In the PAW approach, the pseudo wavefunctions $\tilde{\varphi}_i$ do not obey the orthonormality condition, $\langle\tilde{\varphi}_i|\tilde{\varphi}_j\rangle \neq 0$. Nevertheless they fulfill the orthogonality condition

$$\langle\tilde{\varphi}_i|\tilde{S}|\tilde{\varphi}_j\rangle = \delta_{ij}, \tag{5.23}$$

where the overlap operator $\tilde{S}$ can be defined as

$$\tilde{S}[\{\mathbf{R}\}] \;=\; \hat{\mathcal{T}}^{\dagger}\hat{1}\hat{\mathcal{T}} \;=\; 1+\sum_i |\tilde{p}_i\rangle\, q_{ij}\, \langle\tilde{p}_i|\,, \tag{5.24}$$

with $q_{ij} = \langle\xi_i|\xi_j\rangle - \langle\tilde{\xi}_i|\tilde{\xi}_j\rangle$.

5.3.2 Kohn-Sham Equations

Within the PAW formalism, the Kohn-Sham equations can be written as

$$\tilde{H}\tilde{\varphi}_i \;=\; \tilde{\epsilon}_i\tilde{S}\tilde{\varphi}_i. \tag{5.25}$$

This equation looks rather simple to implement and use, in spite of being a generalized eigenvalue problem. Unfortunately, the Hamiltonian operator changes as well in the PAW formalism. In fact, it has to be derived from the total energy functional (5.19) with respect to the pseudo density operator $\tilde{\rho} = \sum_i f_i\, |\tilde{\varphi}_i\rangle\, \langle\tilde{\varphi}_i|$ (as for a one-particle operator $\langle\hat{O}\rangle = \mathrm{Tr}[\rho\hat{O}]$).
So the Hamiltonian is given by

$$\tilde{H} \;=\; \frac{dE}{d\tilde{\rho}} \;=\; \frac{\partial E}{\partial\tilde{\rho}} + \int d^3r\; \frac{\delta E}{\delta\tilde{n}(\mathbf{r})}\frac{\partial\tilde{n}(\mathbf{r})}{\partial\tilde{\rho}} + \sum_{i,j}\frac{\partial E}{\partial\rho_{ij}}\frac{\partial\rho_{ij}}{\partial\tilde{\rho}} \tag{5.26}$$

where $\frac{\partial\tilde{n}(\mathbf{r})}{\partial\tilde{\rho}} = |\mathbf{r}\rangle\,\langle\mathbf{r})|$ and $\frac{\partial\rho_{ij}}{\partial\tilde{\rho}} = |\tilde{p}_i\rangle\,\langle\tilde{p}_i|$. Three helpful definitions are

$$\tilde{D}_{ij} = \frac{\delta\tilde{E}}{\delta\rho_{ij}}, \qquad D^1_{ij} = \frac{\delta E^1}{\delta\rho_{ij}}, \quad \text{and} \quad \tilde{D}^1_{ij} = \frac{\delta\tilde{E}^1}{\delta\rho_{ij}}. \tag{5.27}$$

Finally, the Hamiltonian can be written as

$$\tilde{H}[\rho,\{\mathbf{R}\}] \;=\; -\frac{\nabla^2}{2} + \tilde{v}_{\mathrm{eff}} + \sum_{ij}|\tilde{p}_i\rangle\,(\tilde{D}_{ij} + D^1_{ij} + \tilde{D}^1_{ij})\,\langle\tilde{p}_i|\,, \tag{5.28}$$

where

$$\tilde{v}_{\mathrm{eff}} = v_{\mathrm{H}}[\tilde{n}+\hat{n}+\tilde{n}_{Zc}] + v_{\mathrm{xc}}[\tilde{n}+\hat{n}+\tilde{n}_c] \tag{5.29}$$

is the usual effective one-electron potential. Here v_{xc} stands for the electronic exchange-correlation potential and v_{H} for the Hartree potential.

5.3.3 Forces

The forces are usually defined as the derivative of the total energy with respect to the ionic positions (1.24). In the PAW method, complications arise from the fact that the augmentation spheres and compensation charges are allowed to move with the ions, which spawn additional terms. Further difficulties emerge from the nuclear position dependence of the overlap operator. Notwithstanding, the forces can be derived in several ways [39, 41]. A simple derivation starts with the force theorem first proven by Goedecker and Maschke which states:

$$\mathbf{F}_i = -\frac{\partial E}{\partial \mathbf{R}_i} = \sum_j f_j \langle \tilde{\xi}_j | \frac{\partial}{\partial \mathbf{R}_i} \left[\tilde{H}[\rho, \{\mathbf{R}\}] - \epsilon_j \tilde{S}[\{\mathbf{R}\}] \right] | \tilde{\xi}_j \rangle + \frac{\partial U}{\partial \mathbf{R}_i}, \tag{5.30}$$

where the derivative of $U \equiv U(\mathbf{R}_j, Z_i)$ describes the forces between the ionic cores and the index i stands for each nuclei. From this expression results three terms [41]: the first comes from the change of the local potential v_{eff} if the ions are moved, the second contribution arises from $\hat{D}_{ij}$ due to changes of the compensation charges $\hat{n}$ if the ions are moved and the third is due to the change of the projectors $\tilde{p}_{ij}$.

Part IV

Applications

Chapter 6

Methodology

Intuition is more important to discovery than logic.

Henry Poincaré

6.1 Optical and Magnetical Properties

Intuition... As presented in the introduction, the main objective of this work is to find endohedral silicon cages with different structures, due to a different magnetization of the system and then investigate if these different structures can be identified by their photo-absorption spectrum. The contents of the silicon cages vary from atoms to clusters of some transition metals. A special interest is laid on Chromium, Manganese, Iron and Cobalt for their renowned magnetic properties.

Therefore this work can be divided in two parts: Geometry optimization and Photo-absorpion Spectra. The DFT implementation chosen to perform the geometry optimization was the ABINIT code [40, 43, 44] whereas, to calculate the photo-absorption spectra, a real-time TDDFT implementation has been used: the Octopus code [45–47]. Alas, intuition played a vital role in deciding which variables were best to achieve convergence of the SCF cycle. Furthermore, the Generalized Gradient Approximation was adopted in all calculations (for consistency) and the exchange and correlation functional used in this thesis was the

spin-polarized form of the PBE (Perdew, Burke and Ernzerhof) from the Libxc [48], also shown in subsection 2.5.2.

6.2 Geometry optimization with ABINIT

6.2.1 A look into ABINIT

ABINIT is a package whose main program allows one to find the total energy, charge density and electronic structure of systems made of electrons and nuclei. It also includes options to optimize the geometry according to the DFT forces and stresses. It uses a plane-wave basis for the expansion of the Kohn-Sham orbitals (on a Fast Fourier Transform Grid, FFT Grid) and the pseudopotential approximation or the PAW method to decrease the computing time of a simulation.

According to Bloch's theorem (check [49]), the Kohn-Sham orbitals ($\varphi_{i,\mathbf{k}}(\mathbf{r})$) can be written as

$$\varphi_{i,\mathbf{k}}(\mathbf{r}) = \sum_m c_{i,\mathbf{k}}(\mathbf{G}_m) e^{\mathrm{i}(\mathbf{k}+\mathbf{G}_m)\cdot\mathbf{r}} \equiv \sum_m c_{i,\mathbf{k}}(\mathbf{G}_m) \left|\mathbf{k}+\mathbf{G}_m\right\rangle , \tag{6.1}$$

where $\mathbf{k}$ is the wave vector, i the band index and $\mathbf{G}$ represents the reciprocal lattice vectors. According to this transformation, the Kohn-Sham equations may be expressed as

$$\sum_{m'} \hat{H}_{mm'}(\mathbf{k}) c_{i,\mathbf{k}}(\mathbf{G}_{m'}) = \epsilon_{i,\mathbf{k}} c_{i,\mathbf{k}}(\mathbf{G}_m), \tag{6.2}$$

where the Hamiltonian is given by

$$\hat{H}_{mm'} = \left\langle \mathbf{k}+\mathbf{G}_m \right| -\frac{\nabla^2}{2} + v_{\mathrm{KS}} \left|\mathbf{k}+\mathbf{G}_m\right\rangle . \tag{6.3}$$

Therefore, a plane wave expansion is rather good to describe solids, as it takes advantage of the periodicity of the system. Nevertheless, plane waves can also be used to describe atoms and clusters if the super-cell approach is used. In this approach the unit cell (in normal space) is taken to be very big, in order to avoid interactions between neighbouring cells. Then a convergence of the size of the cell, with respect to the energy, has to be made. Basically, one has to increment the size of the cell until the variation of the energy is less than a desired

tolerance. Normally in a plane wave calculation a convergence over the Brillouin zone sampling has also to be made (one has to determine how many k-points are needed to correctly describe the system). Fortunately, as the unit cell has to be very big for finite systems, the reciprocal cell and its Wigner-Seitz cell (the first Brillouin zone) will be very small. As a consequence, only one k-point is necessary ($\mathbf{k} = (0, 0, 0)$). Finally, one last parameter has to be converged, a cutoff radius in reciprocal space to truncate over reciprocal lattice vectors (the sum over m' in (6.2) cannot have infinite terms). In ABINIT this is done by setting a kinetic energy cut-off, which controls the number of planewaves at a given k point, i.e., $\frac{1}{2}[2\pi(\mathbf{k}+\mathbf{G}_{max})]^2$ is the kinetic energy cut-off for the maximum reciprocal vector.

6.2.2 PAW Method

To optimize the geometry of the endohedral silicon cages the PAW method was used. This was indispensable because of the number of the plane waves and the unit cell size, the parameters that have to be fine-tuned in every calculation, were not converging with norm-conserving pseudopotentials (Troullier-Martins for the $3d$ and its extension for the others). Well, good transferability of a Troullier-Martins norm-conserving pseudopotential, requires a core radius around the outer most maximum of the all electron wavefunction. Only then will the pseudo wavefunction correctly describe the charge distribution and moments of the all electron wavefunction. Therefore, for elements with strongly localized orbitals (like the $3d$ orbitals of the transition metals), the resulting norm-conserving pseudopotentials require a large plane-wave basis set. Whereas the PAW method presents an elegant solution for this method.

The basic changes to the Kohn-Sham equations can be found in chapter 5, as well as details on how the energy and the forces are calculated. This can also be found in [40], which describes how the PAW method was implemented in ABINIT. In order to use this method, one needs PAW datasets, which provides the informations about the PAW functions. More information on the PAW datasets used in this thesis can be found in [50]. To transfer data from the normal FFT grid to the spherical grid around each atom (PAW partial wave grid) another grid is needed, a "double grid" which is basically a fine FFT grid. As a consequence,

on more convergence parameter is added to the calculation, which is basically the kinetic energy cut-off for this double grid. This parameter has to be bigger or equal to the kinetic energy cut-off on the normal grid.

6.2.3 Geometry Optimization

At last, to optimize a geometry for a spin-polarized case, one has to solve self-consistently the Kohn-Sham equations of subsection 2.4.1 and calculate the energy and the forces, using the Hellmann-Feynman theorem (1.24). Then minimization of the energy with respect to the nuclear coordinates will find the geometry where the forces are smaller. In every minimization step, the Kohn-Sham equations have to be solved again. To find the optimized geometries of the endohedral silicon cages in this thesis, the Broyden-Fletcher-Goldfarb-Shanno minimization [51] was used.

6.3 Photo-absorpion Spectra with Octopus

6.3.1 A look into Octopus

Octopus is a scientific program aimed at the *ab initio* virtual experimentation on a hopefully ever-increasing range of system types. Electrons are described quantum-mechanically within DFT, in its time-dependent form (TDDFT) when doing simulations in time. Nuclei are described classically as point particles and the electron-nucleus interaction is described within the pseudopotential approximation. With Octopus, functions are not expanded in a basis set, but sampled in a real-space mesh or grid [52]. Therefore, the Hartree potential can be obtained by solving the Poisson equation and the kinetic energy can be evaluated by a finite difference method of the form

$$\nabla^2\varphi(\mathbf{r}_i) = \sum_j c_j\varphi(\mathbf{r}_j). \tag{6.4}$$

It is also necessary to define a finite domain of the real space for the simulation. This domain or simulation box can have many forms and its boundary can be subjected to different conditions. For finite systems, like atoms, the wavefunctions

and the density are forced to be zero over the boundary of the domain. As a consequence, there are two parameters that have to be fine-tuned against the results in a real-space calculation, the grid spacing and the simulation box size.

6.3.2 Pseudopotentials and APE

The norm-conserving pseudopotentials used with Octopus in this thesis were obtained with the Atomic Pseudopotentials Engine (APE) [36] as presented in section 4 with a slight difference. In order to include some important relativistic effects in the pseudopotentials, the Dirac's like Kohn-Sham equations of subsection 2.4.2 were used to calculate the all electron wavefunction instead of the Schrödingers' like Kohn-Sham equation. As a consequence, all the equations in section 4.3 are different, but the procedure is the same (for more information check [36]). A relativistic Troullier-Martins scheme and its extension to incorporate semicore states in the valence space were used to construct the pseudo wavefunctions of the transition metals used. The silicon pseudopotential only uses the Troullier-Martins scheme. Ideally, the PAW datasets used for the geometry optimization should have been used here again, instead of the Troullier-Martins pseudopotentials. However, Octopus does not have an implementation of PAW. As the possibilities given by Octopus for the calculation of the spectra were far more that those in other codes (e.g., non-collinear spin), the PAW datasets were used exclusively to obtain a well-relaxed geometry.

6.3.3 Photo-absorption Spectra

The photo-absorption spectra presented in this thesis were obtained using the time-propagation method, as it is implemented in Octopus and described in section 3.5.3, for the spin-polarized Kohn-Sham equations though. The simulation box was chosen to be composed of spheres around each atom and the spacing and the radius chosen for each simulation were the minimum values that converged the spectra (a smaller spacing or a bigger radius would not alter the position of the peaks in the absorption spectra).

6.4 Overall Procedure

The overall work procedure for each transition metal can be summarized as follows:

1. Find an initial geometry.
   The initial geometries were based on the ones found in [4] and [6]. They were reproduced on Avogadro [53] without using any numerical value.

2. Converge the total energy with respect to kinetic energy cut-off, PAW kinetic energy cut-off and cell size in ABINIT.
   These convergence studies showed that a kinetic energy cut-off of 60 Ha and a PAW kinetic energy cut-off of 80 Ha were required to converge the total energy of all the structures. For a cubic cell, the convergence of the total energy, showed that a cell size of 28 bohr were required.

3. Converge the spectra with respect to simulation box radius and grid spacing in Octopus.
   These convergence studies, done with an unoptimized geometry, showed that a radius of 8.0Å and a spacing of 0.10Å were required to converge the spectra. When a SCF calculation had to be performed, the convergence tolerance was the relative density (the cycle would converge when the difference between the input and the output density was less than 1×10^{-7}).

4. Optimize geometry for a certain magnetization.
   Some autonomy was given to ABINIT for the first geometry. Nevertheless, when problems occurred or when optimizing the second magnetization, the magnetization was held fixed. The minimization algorithm would only stop when the greatest force became smaller than 2.5×10^{-3} eV/ Å. In every step of the minimization algorithm a SCF cycle had to be performed to obtain the energy. This cycle would only converge when the difference between the input and the output forces would be less than 2.5×10^{-4} eV/ Å. Optimization with PAW in Abinit proved to be quicker than a geometry optimization with the created norm-conserving pseudopotentials. While a calculation with the $NiSi_{12}$ silicon cage requires a kinetic energy cut-off of

60 Ha with the PAW, with the norm-conserving pseudopotentials this value would have to be higher than 90 Ha. Which would be more computationally demanding, as more planewaves would be needed.

5. Calculate the photo-absorption spectrum for that geometry.

6. Repeat from 4. for another magnetization.

Chapter 7

Silicon cages with one transition metal atom

Science, my lad, is made up of mistakes, but they are mistakes which it is useful to make, because they lead little by little to the truth.

Jules Verne

7.1 Results and discussion

In this chapter, the geometries and the photo-absorption spectra obtained for one transition atom inside a silicon cage are presented. It was intended to present these properties for different magnetizations of 12 transition metal atoms: from Titanium to Copper (check the period in the periodic Table), Palladium, Platinum, Silver and Gold. At the time this thesis was delivered, only 8 atoms were studied (plus Zirconium). For five of these, different structures are shown, one for each different magnetization of the silicon cage. At last, the optical absorption spectra are presented for different magnetizations of Chromium, Manganese, Iron and Cobalt (which were the most interesting).

7.1.1 Optimized geometries

The geometries obtained after the optimization are presented in here. These geometries are divided based on the group of the Periodic Table to which the

encapsulated transition metal atom belongs to.
For each geometry shown there is a column in a posterior table where some properties of the geometry are presented. These properties are the symmetry group, the value of the magnetic moment m_z and the total energy. As in section 2.4.1 the total magnetic moment is related to m_z, $\mathbf{m} = (0, 0, m_z)$). The values of these properties should be treated with care, and should not be considered as absolute. For example, the total energy was obtained for a given valence and for the PBE functional, so it might change if calculated with other functional. Regardless, differences, like the magnetic moment, will not change.

The geometries for the Cr, Mn, Fe and Co cages are shown in a different way. Instead of showing all the bonds (every silicon interacts with the atom inside), only a fraction of these bond lengths is shown. This permits to better identify the silicon atoms that are closer to the transition metal, and which silicon atoms are closer to one another.

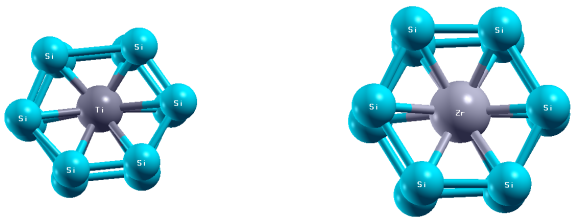

(A) $TiSi_{12}$ with $m_z = 0$. (B) $ZrSi_{12}$ with $m_z = 0$.

FIGURE 7.1: Optimized geometries for the cages encapsulating a group four transition metal atom.

Property	$TiSi_{12}$	$ZrSi_{12}$
Symmetry	Distortion of D_{6h}	Distortion of D_{6h}
m_z	0	0
Total Energy / Ha	-106.12	-94.96

TABLE 7.1: Some properties of the geometries presented in figure 7.1

.

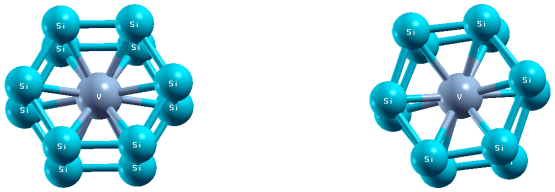

(A) VSi_{12} with $m_z = 1$. (B) VSi_{12} with $m_z = 3$.

FIGURE 7.2: Optimized geometries for the cages encapsulating a group five transition metal atom.

Property	VSi_{12}	VSi_{12}
Symmetry	D_{6h}	D_{6h}
m_z	1	3
Total Energy / Ha	-119.57	-119.53

TABLE 7.2: Some properties of the geometries presented in figure 7.2.

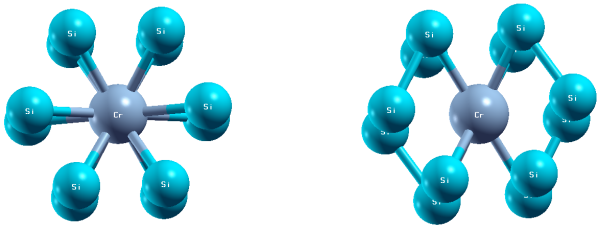

(A) $CrSi_{12}$ with $m_z = 0$. (B) $CrSi_{12}$ with $m_z = 2$.

FIGURE 7.3: Optimized geometries for the cages encapsulating a group six transition metal atom.

Property	$CrSi_{12}$	$CrSi_{12}$
Symmetry	D_{6h}	D_{6h}
m_z	0	0
Total Energy / Ha	-134.92	-134.90

TABLE 7.3: Some properties of the geometries presented in figure 7.3.

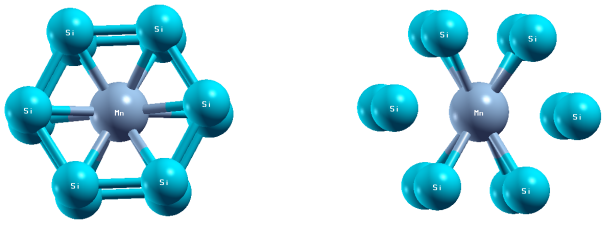

(A) $MnSi_{12}$with $m_z = 1$. (B) $MnSi_{12}$with $m_z = 3$.

FIGURE 7.4: Optimized geometries for the cages encapsulating a group seven transition metal atom .

Property	$MnSi_{12}$	$MnSi_{12}$
Symmetry	D_{6h}	D_{6h}
m_z	1	0
Total Energy /Ha	-152.34	-152.30

TABLE 7.4: Some properties of the geometries presented in figure 7.4.

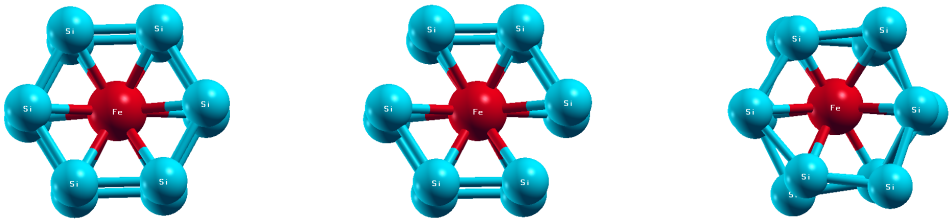

(A) $FeSi_{12}$ with $m_z = 0$. (B) $FeSi_{12}$ with $m_z = 2$. (C) $FeSi_{12}$ with $m_z = 4$.

FIGURE 7.5: Optimized geometries for the cages encapsulating a group nine transition metal atom.

Property	$FeSi_{12}$	$FeSi_{12}$	$FeSi_{12}$
Symmetry	D_{6h}	D_{6h}	Distortion of D_{6h}
m_z	0	2	4
Total Energy / Ha	-171.95	-171.94	-171.91

TABLE 7.5: Some properties of the geometries presented in figure 7.5.

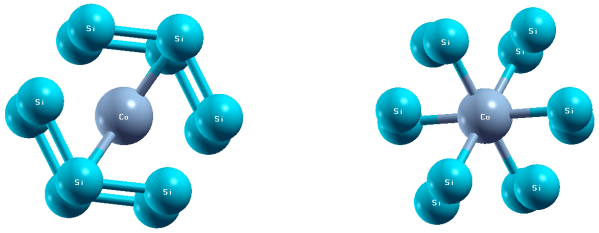

(A) $CoSi_{12}$ with $m_z = 1$. (B) $CoSi_{12}$ with $m_z = 3$.

FIGURE 7.6: Optimized geometries for the cages encapsulating a group nine transition metal atom.

Property	$CoSi_{12}$	$CoSi_{12}$
Symmetry	D_{6h}	Distortion of D_{6h}
m_z	1	3
Total Energy / Ha	-193.91	-193.89

TABLE 7.6: Some properties of the geometries presented in figure 7.6.

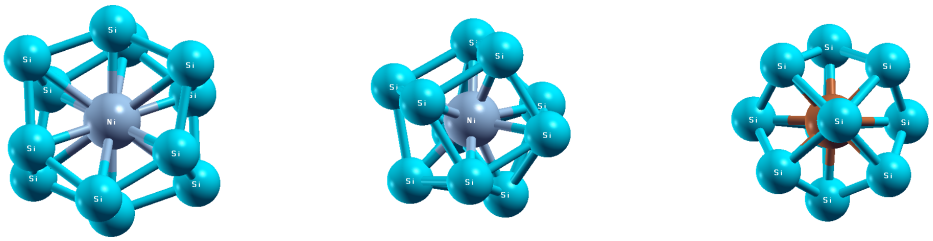

(A) $NiSi_{12}$ with $m_z = 2$. (B) $NiSi_{10}$ with $m_z = 0$. (C) $CuSi_{10}$ with $m_z = 1$.

FIGURE 7.7: Optimized geometries for the cages encapsulating a group ten or eleven transition metal atom.

Property	$NiSi_{12}$	$NiSi_{10}$	$CuSi_{10}$
Symmetry	Distortion of D_{6h}	Distortion of D_{4d}	Distortion of D_{4d}
m_z	2	0	1
Total Energy / Ha	-218.36	-210.47	-237.50

TABLE 7.7: Some properties of the geometries presented in figure 7.7.

As can be seen in the last figures and tables, the geometries depend on the atom that is inside the silicon cage, but for atoms close in the periodic table, these cages show similar structures. All structures with 12 silicon atoms are similar. One atom between two layers of silicon. And each layer of silicon forms an hexagon.

Furthermore, the magnetic moment has some small influence in the geometry and in the energy of the cage. The energies presented above for the same type of atom inside the silicon cage show that the higher the magnetization, the

smaller the energy. Well, the biggest difference between energies of geometries with different magnetic moment is 0.04 Ha = 1.09 eV in 171.9 Ha for the Iron cages. Besides, the magnetic moment also change the distance between atoms. But once again the changes are small. For the Manganese $m_z = 1$ cage in figure 7.4, the distance between the Manganese and the silicon atoms is approximately 2.61Å for all silicon atoms, while the distance between silicon atoms is 2.36Å. For the $m_z = 3$, the distance between the silicon atoms and the Manganese can take two values, 2.59Å and 2.70Å (for the atoms that do not share a bond only in the figure). These silicon atoms also get further away from the opposite layer of silicon atoms.

7.1.2 Photo-absorption Spectra

Figure 7.8 shows the photo-absorption spectra obtained.

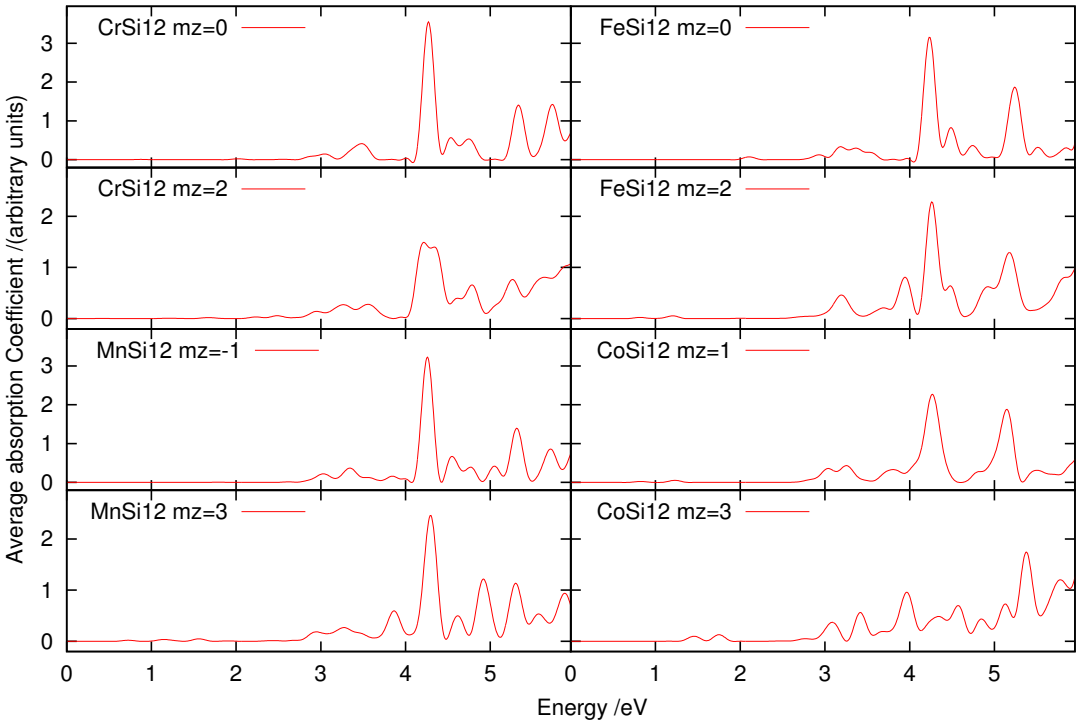

FIGURE 7.8: Photo-absorption spectrum for the endohedral silicon cages containing one atom of Cr, Mn, Fe and Co for two different magnetizations.

Due to a distraction, the results presented in figure 7.8 were obtained with the Slater exchange (LDA) and the modified Perdew & Zunger correlation functionals (octopus default). Luckily the results for the PBE (GGA)are similar, as can be seen in figure 7.9 for the $CrSi_{12}$ endohedral silicon cage.

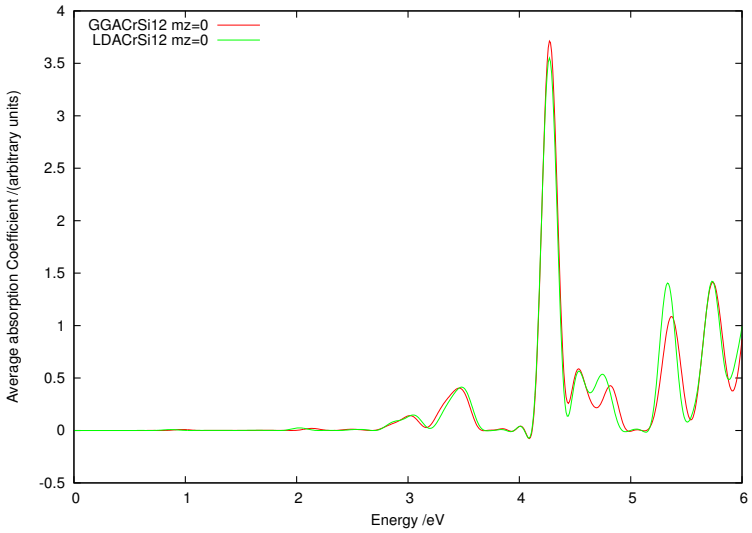

FIGURE 7.9: Photo-absorption Spectra for $CrSi_{12}$. Obtained using the default LDA from octopus and the PBE (GGA).

Before analysing the spectra, one first has to determine the ionization threshold. Above this energy limit, the electrons leave the atom and are no longer correctly described. As such, above this threshold the spectra are no longer reliable. The ionization potentials, calculated from $I = -\epsilon_{max}$, are presented in table 7.8, the eigenvalues used were the ones calculated by Octopus during the calculation of the ground state.

Cage	m_z	I / eV	m_z	I / eV
$CrSi_{12}$	0	5.689	2	5.775
$MnSi_{12}$	1	5.754	3	4.226
$FeSi_{12}$	0	4.586	2	4.1612
$CoSi_{12}$	1	4.166	3	4.717

TABLE 7.8: Ionization potentials for the Cr, Mn, Fe and Co endohedral silicon cages.

This might not be the correct way to calculate the ionization potential, as LDA and most GGA are known to be unreliable for describing the ionization process, mainly because of a incorrect asymptotic behaviour. For a better ionization potential one should also calculate the energy of the system without one electron and subtract both. Nevertheless, for transitions which are greater than the highest occupied molecular orbital, the excited state is not well described (LDA and GGA incorrect asymptotic behaviour strikes again). Then to study the spectra presented above, one should restrict the analysis to energy values lower the 5 eV.

The atoms inside the cages whose spectrum was presented in figure 7.8, have similar properties: they all belong to the same period of the Periodic Table and they are all known for their magnetic properties. Hence their interest in this thesis.

At first sight, all the spectra show resemblances. Obviously, the transition metal atom inside the cage contributes for the optical properties of the combined system (the endohedral cage), due to its own electronic structure, to the bonds with the silicon atoms and because its location inside the cage changes the system geometry. Nevertheless, all geometries share a similar silicon cage (formed by 12 silicon atoms disposed in two superposing hexagons). And, probably because of that, all geometries share a characteristic peak around 4.2 eV. The intensity of these peaks vary with the magnetization of the endohedral cage. As shown in the last figure, when the difference of the spin-up and spin-down valence electrons is increased, the intensity of this peak diminishes. Also, the cobalt cages show the least intense peaks. Near those 4.2 eV peaks, one can distinguish at least two more lesser peaks. Table 7.9 shows their energies and between parentheses their relative intensities.

Cage	First	Second	Third	Fourth
$CrSi_{12}$ ($m_z = 0$)	4.01(0.05)	4.26(3.54)	4.54(0.58)	4.71(0.54)
$CrSi_{12}$ ($m_z = 2$)	4.21(1.49)	4.33(1.41)	4.60(0.41)	4.79(0.66)
$MnSi_{12}$ ($m_z = 1$)	3.83(0.15)	4.26(3.21)	4.55(0.66)	4.77(0.40)
$MnSi_{12}$ ($m_z = 3$)	3.87(0.60)	4.29(2.46)	4.11(0.49)	4.90(1.22)
$FeSi_{12}$ ($m_z = 0$)	3.97(0.03)	4.23(3.14)	4.48(0.83)	4.73(0.37)
$FeSi_{12}$ ($m_z = 2$)	3.94(0.83)	4.26(2.29)	4.48(0.63)	4.91(0.63)
$CoSi_{12}$ ($m_z = 1$)	3.26 (0.44)	3.80(0.33)	4.26(2.27)	
$CoSi_{12}$ ($m_z = 3$)	3.41(0.55)	3.66(0.20)	3.96(0.96)	4.33(0.48)

TABLE 7.9: Predominant peaks for the Cr, Mn, Fe and Co endohedral silicon cages.

A closer look at the last table and at the spectra, shows how one can try to differentiate two different magnetizations of the same cage based on different intensities. As seen before, the lenght of the peak around 4.2 eV is always larger for the least magnetization. Then, before that peak, there is one smaller peak which is greater, the greater the magnetization. Finally, after the 4.2 eV transition peak, there is always another peak, which has greater intensity if the magnetization is smaller. An exception is the cobalt cage with $m_z = 3$. If one looks at its structure in figure 7.6 it is easy to understand why the spectrum does not behave like the others: the D_{6h} symmetry is very distorted, almost at a breaking point, like the Iron geometry for $m_z = 4$ (both these geometries were optimized until no force were greater done 2.5×10^{-3} eV/ Å, though). While the spectra in figure 7.8 might look distinguishable in an analysis based on peak intensities, in a real spectroscopy experiment, that might not be the case, due to impurities or to the machinery to measure. Based on that, one should rather look at the number of peaks and at their relative position (the theoretical spectra have almost always their peaks shifted relatively to the peaks of the experimental spectra).

Then, what follows, is a careful analysis of the spectra for each atom. For Chromium, the spectrum for the cage with $m_z = 0$ has no peaks until 3 eV. Around this value, there are two close peaks and then there is another peak at roughly 3.5 eV. Afterwards there is the big peak around 4.2 eV. The spectra for $m_z = 2$ is similar, with no peaks until 3eV, but then it has 3 distinct peaks that

follow one another. The main difference from the former spectrum, is that at 4.2 eV, one can clearly see two peaks.

On the other hand, for Manganese, the spectrum for the geometry with $m_z = -1$ shows no peaks until 3 eV, then presents 5 peaks before the well known 4.2 eV peak. The spectra for the other magnetization appears to have 3 peaks around 1 eV and then four peaks past 3 eV until superior peak.

While for Iron, the spectra with null magnetization shows a small peak around 2 eV and a structure of four close peaks between 2.9 and 3.5 eV. Instead, the spectra for a total magnetic moment of 2 presents a small peak past 1 eV and a bigger one past 3 eV. Then comes the important part, the next two peaks only appears past the 3.5 eV. This shows a change in the response of the system due to a different magnetization.

Finally for Cobalt, there is a gap between the first peaks and the 3 eV peaks. These first peaks appear first for the geometry with less magnetization (around 1 eV). After the 3 eV mark, the geometry with higher magnetization appears to have more peaks. This could be important, a strong magnetization could break the symmetry of a cage without completely destroying it. This could allow the atoms to interact more, which could increase the excitations. At least that is what looks like it is happening with Cobalt. Therefore, an increase in the magnetization can yield an increase in excitation energies.

In conclusion, there are small differences between the geometries with different magnetizations (for the same type of atom inside the cage). These differences can be measured in a displacement of 0.1Å. The changes in the geometry are enough to slightly change the photo-absorption spectra, and some distinctions can be found between spectra for cages with the same type of atom inside. However, part of these differences are based on the relative intensities of the peaks. While the other part are based on peaks whose average orientational absorption coefficient is very small. So, could these cages be used to to construct something useful? Well, if the experimental spectra is as clear as the ones shown in figure 7.8, which is rather improbable, it might. And it would come in handy that the cages' structure do not change that much for a different magnetization. The hypothetical device would even be more compact and durable. Although all of this requires one more property: the system has to be able to change between

magnetizations, when a electrical field is applied. Nonetheless, in practise, with an experimental spectrum, it might not be possible to distinguish between the endohedral silicon cages, with different magnetizations with only one atom inside them. The next step is to place another atom inside the cage. Obviously, it might be necessary to add more silicon atoms to create a stable structure.

Chapter 8

Silicon cages with two transition metal atoms

You can't always get what you want, but if you try sometimes you just might find, you get what you need ...

Rolling Stones

8.1 Results and Discussion

The structures found for the endohedral silicon cages with two transition metal atoms inside are shown in figure 8.1.

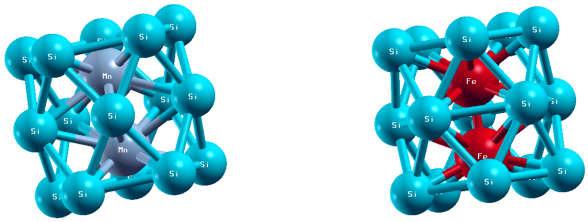

(A) Mn_2Si_{15} with $m_z = 0$. (B) Fe_2Si_{15} with $m_z = 0$.

FIGURE 8.1: Endohedral silicon cage with two transition metal atoms inside. These structures have a D_{5h} symmetry.

Instead of two layers of hexagons, the structure for the silicon cages with two transition metal atoms consist in three layers of silicon atoms, forming a pentagon in each layer. The atoms that form the pair, can be found between them.

Figure 8.2 shows the optical-absorption spectra of the Fe_2Si_{15} silicon cage. For an easy comparison, the optical-absorption spectra for the $FeSi_{12}$ is also presented.

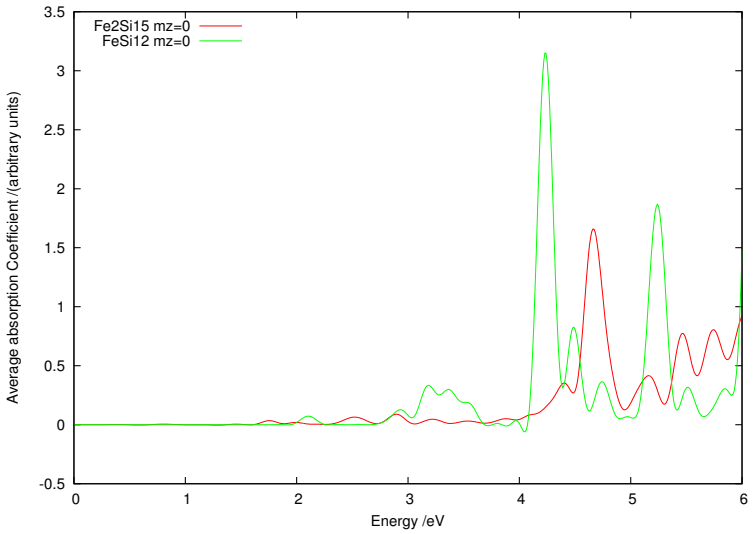

FIGURE 8.2: Comparison between the Fe_2Si_{15} and $FeSi_{12}$ photo-absorption spectra. The highest occupied molecular orbital eigenvalue is -4.90 eV.

The characteristic peak around 4.20 eV is shifted to 4.66 eV (and has lesser intensity). The spectra also appears to have a peak around 2.5 eV and another around 3.0 eV.

Another promising feature of the Fe_2Si_{15} spectrum is small number of peaks, almost like the silicon structure is shielding the atoms (indeed it looks like that in the figure 8.1). This is great because an increase in the magnetization could increase the number of peaks. Then one would have two distinct Iron dimer geometries inside a silicon cage.

Part V

Conclusion

Conclusions

This study of optical and magnetic properties of endohedral silicon cages containing transition metal atoms proved that the photo-absorption spectra obtained using TDDFT can, in theory, identify different magnetic moments of the cages. Unfortunately, for cages encapsulating a single atom, these differences are based on relative intensities or in transitions represented by small peaks. This means that in a spectroscopy experiment, the identification of the structure may prove to be rather difficult.

It was also shown that the relaxed geometry of the silicon cages can be easily obtain with the DFT formalism.

The work is never over, there is always something to do. The results presented in this thesis were not good. A spintronics device can not be envision based on these silicon cages. Mercifully, silicon cages containing two transition atoms (or more) might provide the required properties. Therefore, more studies have to be made concerning the endohedral silicon cages.

References

[1] S. A. Wolf, D. D. Awschalom, R. A. Buhrman, J. M. Daughton, S. von Molnár, M. L. Roukes, A. Y. Chtchelkanova, and D. M. Treger. Spintronics: A spin-based electronics vision for the future. *Science*, 294:1488–1495, Nov 2001. doi: 10.1126/science.1065389. 3

[2] S. Datta and B. Das. Electronic analog of the electro-optic modulator. *Appl. Phys. Lett.*, 56, 1990. doi: 10.1063/1.102730. 3

[3] Micael José Tourdot de Oliveira. *Relativistic effects in the optical response of low-dimensional structures: new developments and applications within a time-dependent density functional theory framework*. PhD thesis, Faculdade de Ciências e Tecnologia da Universidade de Coimbra, 2008. 3, 10, 26, 41

[4] Micael J. T. Oliveira, Paulo V. C. Medeiros, José R. F. Sousa, Fernando Nogueira, and Gueorgui K. Gueorguiev. Optical and magnetic excitations of metal-encapsulating si cages: A systematic study by time-dependent density functional theory. *J. Phys. Chem. C,*, 118 (21):11377–11384, 2014. doi: 10.1021/jp4096562. 4, 70

[5] G.K. Gueorguiev, J.M. Pacheco, S. Stafström, and L. Hultman. Silicon–metal clusters: Nano-templates for cluster assembled materials. *Thin Solid Films*, 515(3):1192 – 1196, 2006. ISSN 0040-6090. doi: http://dx.doi.org/10.1016/j.tsf.2006.07.114. Proceedings of the 33rd International Conference on Metallurgical Coatings and Thin Films {ICMCTF} 2006.

[6] Hung Tan Pham, Thu-Thuy Phan, Nguyen Minh Tam, Long Van Duong, My Phuong Pham-Ho, and Minh Tho Nguyen. Mn2@si15: the smallest triple

ring tubular silicon cluster. *Phys. Chem. Chem. Phys.*, 17:17566–17570, 2015. doi: 10.1039/C5CP02257F. 4, 70

[7] R. M. Martin. *Electronic Structure: Basic Theory and Practical Methods*. Cambridge University Press, 2004. 7, 10

[8] A. Szabo and N.S. Ostlund. *Modern Quantum Chemistry: Introduction to Advanced Electronic Structure Theory*. Dover Books on Chemistry Series. Dover Publications, 1996. 7

[9] Pedro Miguel Monteiro Campos de Melo. Orbital dependent functionals in non-collinear spin systems. Master's thesis, Faculdade de Ciências e Tecnologia da Universidade de Coimbra, 2012. 10

[10] R.G. Parr and W. Yang. *Density-Functional Theory of Atoms and Molecules*. Oxford University Press, Inc., 1989. 12, 15

[11] J.G. Esteve, Fernando Falceto, and C. García Canal. Generalization of the hellmann–feynman theorem. *Physics Letters A*, 374(6):819 – 822, 2010. ISSN 0375-9601. doi: http://dx.doi.org/10.1016/j.physleta.2009.12.005. 13

[12] C. Fiolhais, F. Nogueira, and M. Marques A.L. (Eds.). *A Primer in Density Functional Theory*. Springer-Verlag Berlin Heidelberg, 2003. 15, 24, 50, 51

[13] R. M. Dreizler, E. K. U. Gross, and K. U. Eberhard. *Density Functional Theory: An approach to the Quantum Many-Body Problem*. Springer-Verlag Berlin Heidelberg, 1990. 15, 16

[14] P. Hohenberg and W. Kohn. Inhomogeneous electron gas. *Phys. Rev.*, 136: B864–B871, Nov 1964. doi: 10.1103/PhysRev.136.B864. 16

[15] M. Levy. Universal variational functionals of electron densities, first-order density matrices, and natural spin-orbitals and solution of the v-representability problem. *Proc.Natl.Acad.Sci.U.S.A.*, 76:6062, 1979. 20

[16] W. Kohn and L. J. Sham. Self-consistent equations including exchange and correlation effects. *Phys. Rev.*, 140:A1133–A1138, Nov 1965. doi: 10.1103/PhysRev.140.A1133. 22, 27

[17] Pedro Borlido. Atomic ionization energies with hybrid functionals. Master's thesis, Faculdade de Ciências e Tecnologia da Universidade de Coimbra, 2014. 22

[18] U von Barth and L Hedin. A local exchange-correlation potential for the spin polarized case. *Journal of Physics C: Solid State Physics*, 5(13):1629, 1972. 25

[19] Tiago Cerqueira. Influence of the exchange and correlation functional in the ionization potentials of atoms. Master's thesis, Faculdade de Ciências e Tecnologia da Universidade de Coimbra, 2012. 25

[20] M V Ramana and A K Rajagopal. Theory of spin polarised inhomogeneous relativistic electron gas. *Journal of Physics C: Solid State Physics*, 14(29): 4291. 26

[21] E. Engel, T. Auth, and R. M. Dreizler. Relativistic spin-density-functional theory: Robust solution of single-particle equations for open-subshell atoms. *Phys. Rev. B*, 64:235126, Nov 2001. doi: 10.1103/PhysRevB.64.235126. 26

[22] J. P. Perdew and Alex Zunger. Self-interaction correction to density-functional approximations for many-electron systems. *Phys. Rev. B*, 23: 5048–5079, May 1981. doi: 10.1103/PhysRevB.23.5048. 27

[23] J. P. Perdew, K. Burke, and M. Ernzerhof. Generalized gradient approximation made simple. *Phys. Rev. Lett.*, 77:3865, 1996. 28

[24] J. P. Perdew, K. Burke, and M. Ernzerhof. Generalized gradient approximation made simple. *Phys. Rev. Lett.*, 78:1396, 1997. 28

[25] F. Nogueira A. Rubio K. Burke M.A.L. Marques, C. Ullrich and E.K.U. Gross (Eds.). *Time-dependent density functional theory*. Lecture Notes in Physics, Vol. 706, Springer, Berlin, 2006. 31, 45

[26] F. Nogueira E.K.U. Gross M.A.L. Marques, N.T. Maitra and A. Rubio (Eds.). *Fundamentals of time-dependent density functional theory*. Lecture Notes in Physics, Vol. 837, Springer, Berlin, 2012. 31

[27] Erich Runge and E. K. U. Gross. Density-functional theory for time-dependent systems. *Phys. Rev. Lett.*, 52:997–1000, Mar 1984. doi: 10.1103/PhysRevLett.52.997. 32

[28] Robert van Leeuwen. Causality and symmetry in time-dependent density-functional theory. *Phys. Rev. Lett.*, 80:1280–1283, Feb 1998. doi: 10.1103/PhysRevLett.80.1280. 36

[29] K. L. Liu and S. H. Vosko. A time-dependent spin density functional theory for the dynamical spin susceptibility. *Canadian Journal of Physics*, 67(11): 1015–1021, 1989. doi: 10.1139/p89-178. 37

[30] A. Willets, J.E. Rice, and D.P. Shelton D.M. Burland. problems in the comparison of theoretical and experimental hyperpolarizabilities. *J. Chem. Phys.*, 97:7590–7599, 1992. 39

[31] M.A.L. Marques and E.K.U. Gross. Time-dependent density functional theory. *Annual Review of Physical Chemistry*, 55(1):427–455, 2004. doi: 10.1146/annurev.physchem.55.091602.094449. 42

[32] R. M. Sternheimer. Electronic polarizabilities of ions from the hartree-fock wave functions. *Phys. Rev.*, 96:951–968, Nov 1954. doi: 10.1103/PhysRev.96.951. 44

[33] Mark E. Casida. Time-dependent density-functional theory for molecules and molecular solids. *Journal of Molecular Structure: {THEOCHEM}*, 914(1–3): 3 – 18, 2009. ISSN 0166-1280. doi: http://dx.doi.org/10.1016/j.theochem.2009.08.018. Time-dependent density-functional theory for molecules and molecular solids. 44

[34] K. Yabana and G. F. Bertsch. Time-dependent local-density approximation in real time. *Phys. Rev. B*, 54:4484–4487, Aug 1996. doi: 10.1103/PhysRevB.54.4484. 44

[35] S.J. Singh and L. Nordstrom. *Planewaves, Pseudopotentials and the LAPW Method, 2 Edition*. Springer Science+Business Media, Inc., 2006. 50

[36] Micael J.T. Oliveira and Fernando Nogueira. Generating relativistic pseudo-potentials with explicit incorporation of semi-core states using ape, the atomic pseudo-potentials engine. *Computer Physics Communications*, 178 (7):524 – 534, 2008. ISSN 0010-4655. doi: http://dx.doi.org/10.1016/j.cpc.2007.11.003. 51, 69

[37] D. R. Hamann, M. Schlüter, and C. Chiang. Norm-conserving pseudopotentials. *Phys. Rev. Lett.*, 43:1494–1497, Nov 1979. doi: 10.1103/PhysRevLett.43.1494. 53

[38] N. Troullier and José Luís Martins. Efficient pseudopotentials for plane-wave calculations. *Phys. Rev. B*, 43:1993–2006, Jan 1991. doi: 10.1103/PhysRevB.43.1993. 53

[39] P. E. Blöchl. Projector augmented-wave method. *Phys. Rev. B*, 50:17953–17979, Dec 1994. doi: 10.1103/PhysRevB.50.17953. 55, 62

[40] Marc Torrent, François Jollet, François Bottin, Gilles Zérah, and Xavier Gonze. Implementation of the projector augmented-wave method in the {ABINIT} code: Application to the study of iron under pressure. *Computational Materials Science*, 42(2):337 – 351, 2008. ISSN 0927-0256. doi: http://dx.doi.org/10.1016/j.commatsci.2007.07.020. 55, 65, 67

[41] G. Kresse and D. Joubert. From ultrasoft pseudopotentials to the projector augmented-wave method. *Phys. Rev. B*, 59:1758–1775, Jan 1999. doi: 10.1103/PhysRevB.59.1758. 55, 62

[42] G. Kresse and J. Furthmüller. Efficiency of ab-initio total energy calculations for metals and semiconductors using a plane-wave basis set. *Computational Materials Science*, 6(1):15 – 50, 1996. ISSN 0927-0256. 55

[43] X. Gonze, B. Amadon, P.-M. Anglade, J.-M. Beuken, F. Bottin, P. Boulanger, F. Bruneval, D. Caliste, R. Caracas, M. Côté, T. Deutsch, L. Genovese, Ph. Ghosez, M. Giantomassi, S. Goedecker, D.R. Hamann, P. Hermet, F. Jollet, G. Jomard, S. Leroux, M. Mancini, S. Mazevet, M.J.T. Oliveira, G. Onida, Y. Pouillon, T. Rangel, G.-M. Rignanese, D. Sangalli,

R. Shaltaf, M. Torrent, M.J. Verstraete, G. Zerah, and J.W. Zwanziger. Abinit: First-principles approach to material and nanosystem properties. *Computer Physics Communications*, 180(12):2582 – 2615, 2009. ISSN 0010-4655. doi: 10.1016/j.cpc.2009.07.007. 65

[44] X Gonze, G Rignanese, M Verstraete, J Betiken, Y Pouillon, R Caracas, F Jollet, M Torrent, G Zerah, M Mikami, P Ghosez, M Veithen, J-Y Raty, V Olevano, F Bruneval, R Reining, Land Godby, G Onida, D Hamann, and D Allan. A brief introduction to the abinit software package. 65

[45] X. Andrade, D. A. Strubbe, U. De Giovannini, A. H. Larsen, M. J. T. Oliveira, J. Alberdi-Rodriguez, A. Varas, I. Theophilou, N. Helbig, M. Verstraete, L. Stella, F. Nogueira, A. Aspuru-Guzik, A. Castro, M. A. L. Marques, and A. Rubio. Real-space grids and the octopus code as tools for the development of new simulation approaches for electronic systems. *Physical Chemistry Chemical Physics*, 2015. doi: 10.1039/C5CP00351B. 65

[46] A. Castro, H. Appel, Micael Oliveira, C.A. Rozzi, X. Andrade, F. Lorenzen, M.A.L. Marques, E.K.U. Gross, , and A. Rubio. octopus: a tool for the application of time-dependent density functional theory. *Phys. Stat. Sol. B*, 243:2465–2488, 2006. doi: 10.1002/pssb.200642067.

[47] M.A.L. Marques, Alberto Castro, George F. Bertsch, and Angel Rubio. octopus: a first-principles tool for excited electron-ion dynamics. *Comput. Phys. Commun.*, 151:60–78, 2003. doi: 10.1016/S0010-4655(02)00686-0. 65

[48] Micael J. T. Oliveira Miguel A. L. Marques and Tobias Burnus. Libxc: a library of exchange and correlation functionals for density functional theory. *Comput. Phys. Commun.*, 183:2272–2281, 2012. doi: 10.1016/j.cpc.2012.05.007. 66

[49] N.W. Ashcroft and N.D. Mermin. *Solid State Physics*. Brooks/Cole, 1976. 66

[50] François Jollet, Marc Torrent, and Natalie Holzwarth. Generation of projector augmented-wave atomic data: A 71 element validated table in the

{XML} format. *Computer Physics Communications*, 185(4):1246 – 1254, 2014. ISSN 0010-4655. doi: http://dx.doi.org/10.1016/j.cpc.2013.12.023. 67

[51] J. Nocedal and S. J. Wright. *Numerical Optimization*. Springer New York, 2006. 68

[52] Thomas L. Beck. Real-space mesh techniques in density-functional theory. *Rev. Mod. Phys.*, 72:1041–1080, Oct 2000. doi: 10.1103/RevModPhys.72.1041. 68

[53] Marcus Hanwell, Donald Curtis, David Lonie, Tim Vandermeersch, Eva Zurek, and Geoffrey Hutchison. Avogadro: an advanced semantic chemical editor, visualization, and analysis platform. *Journal of Cheminformatics*, 4 (1):17, 2012. ISSN 1758-2946. doi: 10.1186/1758-2946-4-17. 70